The Astronomical Journal, 131:527–554, 2006 January

UBVRI LIGHT CURVES OF 44 TYPE Ia SUPERNOVAE

Saurabh Jha,[1] Robert P. Kirshner, Peter Challis, Peter M. Garnavich, Thomas Matheson, Alicia M. Soderberg, Genevieve J. M. Graves, Malcolm Hicken, João F. Alves, Héctor G. Arce, Zoltan Balog, Pauline Barmby, Elizabeth J. Barton, Perry Berlind, Ann E. Bragg, César Briceño, Warren R. Brown, James H. Buckley, Nelson Caldwell, Michael L. Calkins, Barbara J. Carter, Kristi Dendy Concannon, R. Hank Donnelly, Kristoffer A. Eriksen, Daniel G. Fabricant, Emilio E. Falco, Fabrizio Fiore, Michael R. Garcia, Mercedes Gómez, Norman A. Grogin, Ted Groner, Paul J. Groot, Karl E. Haisch, Jr., Lee Hartmann, Carl W. Hergenrother, Matthew J. Holman, John P. Huchra, Ray Jayawardhana, Diab Jerius, Sheila J. Kannappan, Dong-Woo Kim, Jan T. Kleyna, Christopher S. Kochanek, Daniel M. Koranyi, Martin Krockenberger, Charles J. Lada, Kevin L. Luhman, Jane X. Luu, Lucas M. Macri, Jeff A. Mader, Andisheh Mahdavi, Massimo Marengo, Brian G. Marsden, Brian A. McLeod, Brian R. McNamara, S. Thomas Megeath, Dan Moraru, Amy E. Mossman, August A. Muench, Jose A. Muñoz, James Muzerolle, Orlando Naranjo, Kristin Nelson-Patel, Michael A. Pahre, Brian M. Patten, James Peters, Wayne Peters, John C. Raymond, Kenneth Rines, Rudolph E. Schild, Gregory J. Sobczak, Timothy B. Spahr, John R. Stauffer, Robert P. Stefanik, Andrew H. Szentgyorgyi, Eric V. Tollestrup, Petri Väisänen, Alexey Vikhlinin, Zhong Wang, S. P. Willner, Scott J. Wolk, Joseph M. Zajac, Ping Zhao, and Krzysztof Z. Stanek

Harvard-Smithsonian Center for Astrophysics, 60 Garden Street, Cambridge, MA 02138; saurabh@astron.berkeley.edu

Received 2004 December 6; accepted 2005 September 3

ABSTRACT

We present *UBVRI* photometry of 44 Type Ia supernovae (SNe Ia) observed from 1997 to 2001 as part of a continuing monitoring campaign at the Fred Lawrence Whipple Observatory of the Harvard-Smithsonian Center for Astrophysics. The data set comprises 2190 observations and is the largest homogeneously observed and reduced sample of SNe Ia to date, nearly doubling the number of well-observed, nearby SNe Ia with published multicolor CCD light curves. The large sample of *U*-band photometry is a unique addition, with important connections to SNe Ia observed at high redshift. The decline rate of SN Ia *U*-band light curves correlates well with the decline rate in other bands, as does the $U - B$ color at maximum light. However, the *U*-band peak magnitudes show an increased dispersion relative to other bands even after accounting for extinction and decline rate, amounting to an additional ~40% intrinsic scatter compared to the *B* band.

Key words: supernovae: general — techniques: photometric

Online material: machine-readable tables

1. INTRODUCTION

Over the last decade, Type Ia supernovae (SNe Ia) have become increasingly sharp tools for precision cosmology, with applications of these exquisite distance indicators ranging from our galactic neighbors to establish the Hubble constant, to halfway across the observable universe to uncover cosmic deceleration and acceleration (Riess et al. 2004; Barris et al. 2004; Knop et al. 2003; and references therein). These cosmological applications of SNe Ia rely on accurate, high-precision, unscheduled measurements of their light curves in multiple passbands over a period of weeks, presenting a challenge to would-be observers.

The project of collecting a large sample of nearby SNe Ia with high-quality, multicolor CCD photometry to be used in cosmological studies began in earnest in 1990 with the Calán/Tololo survey (Hamuy et al. 1993), which combined a photographic search for SNe in the southern sky with a program of CCD follow-up photometry obtained with the help of visiting astronomers. Hamuy et al. (1996b) present Johnson/Cousins *BVI* photometry of 29 SNe Ia from this project (27 of which were discovered as part of the survey itself) out to redshifts $z \simeq 0.1$.

In 1993 astronomers at the Harvard-Smithsonian Center for Astrophysics (CfA) began a campaign of CCD photometric and spectroscopic monitoring of newly discovered SNe at the Fred Lawrence Whipple Observatory (FLWO) on Mount Hopkins in southern Arizona, and this program has been ongoing ever since. We employ a similar cooperative observing strategy for the follow-up photometry, whereby the SN monitoring program is allocated a small amount of time each night (~20 minutes), with the observations being carried out by the scheduled observer. Our SN program is also allocated approximately one dedicated night per month for photometry of the fainter objects, photometric calibration of the SN fields, and template observations after the SNe have faded.

Our cooperative observing strategy has been very successful so far. FLWO *BVRI* observations of 22 SNe Ia discovered between 1993 and 1996 have been published by Riess et al. (1999), and we have also undertaken *UBVRI* photometry and in-depth analysis of a number of individual SNe Ia observed as part of this program: SN 1998bu (Jha et al. 1999), SN 1999by (Garnavich et al. 2004), SN 1998aq (Riess et al. 2005), and SN 2001V (K. Mandel et al. 2006, in preparation).

[1] Current address: Department of Astronomy and Miller Institute for Basic Research, 601 Campbell Hall, University of California, Berkeley, CA 94720-3411.

Here we report our *UBVRI* photometry for 44 SNe Ia discovered between 1997 and 2000. The full data set presented here consists of 2190 observations on 338 nights and is the largest set of homogeneously observed and reduced SN Ia data published to date.

2. DATA AND REDUCTION

2.1. *Discovery*

Our program of SN photometry consists solely of follow-up; we search only our e-mail, not the sky, to find new SNe. A number of observers, both amateur and professional, are engaged in searching for SNe. We rely on these searches, as well as prompt notification of candidates, coordinated by D. Green and B. Marsden of the IAU's Central Bureau for Astronomical Telegrams (CBAT), with confirmed SNe reported in the IAU Circulars. In some cases the SN discoverers provide spectroscopic classification of the new objects, but generally spectroscopy is obtained by others and reported separately in the IAU Circulars. With our spectroscopic SN follow-up program at the FLWO 1.5 m telescope and FAST (Fabricant et al. 1998), we have classified a large fraction of the new, nearby SNe reported over the last several years and compiled a large spectroscopic database (T. Matheson et al. 2006, in preparation).

Given a newly discovered and classified SN, several factors help determine whether or not we include it in our monitoring program. Because of their importance, SNe Ia are often given higher priority over other types, but factors such as ease of observability (southern targets and those discovered far to the west are less appealing), SN phase (objects whose spectra indicate they are after maximum light are given lower priority), and redshift (closer objects are favored), as well as the number of objects we are already monitoring, are significant. Our final sample of well-observed SNe Ia is not obtained from a single well-defined set of criteria, and selection effects in both the searches and follow-up may make this sample unsuitable for some applications (such as determining the intrinsic luminosity function of SNe Ia, for example). A thorough discussion of the selection biases in the Calán/Tololo Supernova Search and follow-up campaign can be found in Hamuy & Pinto (1999).

The discovery data for the sample of SNe Ia presented here are given in Table 1. All the SNe Ia listed were discovered with CCD images, except for SN 1997bp, which was discovered visually, and SN 1999ef and SN 1999gh, which were discovered photographically. New, systematic CCD SN searches have provided the great majority of our sample: the Beijing Astronomical Observatory Supernova Survey (Li et al. 1996; designated as BAO in Table 1), the UK Nova/Supernova Patrol (Armstrong & Hurst 1996; UK), the Puckett Observatory Supernova Search (Puckett 1998; POSS), the Tenagra Observatories Supernova Patrol (Schwartz 1997; TO), and the Lick Observatory Supernova Search (Treffers et al. 1997; LOSS). In addition, we note in Table 1 SNe whose classification as Type Ia is from our spectroscopic monitoring program described above (designated as CfA).

2.2. *Observations*

All the photometry presented here was obtained with the FLWO 1.2 m telescope, with either the AndyCam CCD camera or the 4Shooter 2×2 CCD mosaic (A. Szentgyorgyi et al. 2006, in preparation). Both instruments use thinned, back-side-illuminated, antireflective-coated Loral 2048[2] CCD detectors, situated at the f/8 Cassegrain focus. The pixel scale is approximately $0\farcs33$ pixel^{-1}, yielding a field of view of over $11'$ on a side for each chip. All the data were taken in a 2×2 binned mode, resulting in a sampling of $0\farcs66$ pixel^{-1} that is well matched to the typical image quality ($1\farcs5$–$2''$ FWHM). We have ensured that all data used are within the linear regime of the detectors. Observations using the 4Shooter taken before 1998 October were made with the chip 1 CCD detector, while those taken afterward were made on chip 3, which has slightly improved quantum efficiency (QE) but slightly inferior cosmetic characteristics.

Both instruments have good near-ultraviolet and near-infrared response, and our observations have been in the Johnson *UBV* and Kron-Cousins *RI* bandpasses. The data were taken with two *UBVRI* filter sets, the SAO set and the newer Harris set. Observations before 1998 December were taken with the SAO filter set (the same described by Riess et al. [1999] and Jha et al. [1999]), while those after 1999 May were taken with the Harris set. Between 1998 December and 1999 May only the Harris *UBVR* filters were available, and the *I* filter used was from the SAO filter set. Because of the importance of knowing precisely the bandpasses used for a given observation (particularly for SN photometry), we discuss these in greater detail in § 2.4.

Our observing approach, combining nightly requests for one or two objects with monthly dedicated nights, allows us to sample the light curves with the appropriate cadence. Generally, observations are more frequent when the SNe Ia are near maximum light and less frequent (but deeper) as each SN Ia fades. During the period of these observations, the FLWO 1.2 m was equipped with the 4Shooter or AndyCam usually only during dark time, with an infrared imager on the telescope when the Moon was near full. This unfortunately led to $\sim$1–2 week gaps in our light curves, but in most cases the light curves are still well defined and suitable for distance analyses.

2.3. *Differential Photometry*

To measure the brightness of the SN in any image, we perform the photometry differentially with respect to stars in the field of view, allowing for useful measurements even in nonphotometric conditions. In general we use as many of these comparison stars (or "field standards") as feasible, choosing stars that are bright enough to be precisely measured but faint enough to not saturate the detector in the late-time, deeper images. In addition, we try to choose comparison stars that cover a range of color comparable to those exhibited by SNe Ia over their evolution, although it is often not possible to find stars in the field that are as blue as SNe Ia at or before maximum light. Figure 1 shows *R*-band finder charts for all the SNe and their associated comparison stars.

All the CCD observations were reduced uniformly, with bad-pixel masking, bias subtraction, and flat-field correction using the NOAO Image Reduction and Analysis Facility (IRAF) CCDPROC package.[2] In addition, we remove, to the extent possible, the small but nonnegligible amount of fringing for observations in the *I* band via a fringe frame created from combined night-sky exposures of sparse fields.

A major complication in SN photometry arises in separating light from the SN itself from light from the underlying galaxy at the SN position. Poor subtraction of the background light can have significant effects on the SN light-curve shapes and colors (see the discussions in Riess et al. [1999] and Boisseau & Wheeler [1991]). For this reason, we take observations of the SN fields the following year, after the SN has faded, to use as templates that are subtracted from all the previous images. We have

[2] IRAF is distributed by the National Optical Astronomy Observatory, which is operated by the Association of Universities for Research in Astronomy, Inc., under cooperative agreement with the National Science Foundation.

TABLE 1
SN Ia Discovery and Classification Data

SN Ia	Galaxy	Discovery Date	Discoverer	IAU Circ.	Spectroscopic ID	IAU Circ.
1997E.....	NGC 2258	1997 Jan 14.5	R. Kushida	6538	P. Garnavich & R. Kirshner (CfA)	6538
1997Y.....	NGC 4675	1997 Feb 2	W. Li et al. (BAO)	6556	A. Filippenko et al., P. Garnavich et al. (CfA)	6557
1997bp.....	NGC 4680	1997 Apr 6.5	R. Evans	6613	M. Phillips et al.	6613
1997bq.....	NGC 3147	1997 Apr 8.0	S. Laurie (UK)	6616	P. Challis (CfA)	6616
1997br.....	ESO 576-40	1997 Apr 10.6	Q. Qiao et al. (BAO)	6623	Q. Qiao et al.	6623
1997cn.....	NGC 5490	1997 May 14.6	W. Li et al. (BAO)	6661	M. Turatto et al.	6667
1997cw.....	NGC 105	1997 Jul 10.8	Q. Qiao et al. (BAO)	6699	Q. Qiao et al.	6699
1997dg.....	Anonymous	1997 Sep 27.7	Q. Qiao et al. (BAO)	6749	S. Jha et al. (CfA)	6749
1997do.....	UGC 3845	1997 Oct 31	Y. Qiu et al. (BAO)	6766	Y. Qiu et al.	6766
1997dt	NGC 7448	1997 Nov 22.4	Q. Qiao et al. (BAO)	6775	Q. Qiao et al.	6775
1998D.....	NGC 5440	1998 Jan 28.9	Y. Qiu et al. (BAO)	6815	Y. Qiu et al.	6815
1998V.....	NGC 6627	1998 Mar 12.1	M. Armstrong (UK)	6841	S. Jha et al. (CfA)	6844
1998ab.....	NGC 4704	1998 Apr 1.7	J. Wei et al. (BAO)	6858	P. Garnavich et al. (CfA)	6858
1998bp.....	NGC 6495	1998 Apr 29.1	M. Armstrong (UK)	6890	F. Patat & M. Maia	6890
1998co.....	NGC 7131	1998 Jun 21	W. Johnson	6950	P. Garnavich et al. (CfA)	6950
1998de.....	NGC 252	1998 Jul 23	M. Modjaz et al. (LOSS)	6977	P. Garnavich et al. (CfA)	6980
1998dh.....	NGC 7541	1998 Jul 20.5	W. Li et al. (LOSS)	6978	P. Garnavich et al. (CfA)	6980
1998dk.....	UGC 139	1998 Aug 19.4	J. King et al. (LOSS)	6991	A. Filippenko	6997
1998dm	MCG −01-4-44	1998 Aug 22.5	M. Modjaz et al. (LOSS)	6993	A. Filippenko	6997
1998dx.....	UGC 11149	1998 Sep 10.2	M. Modjaz et al. (LOSS)	7011	S. Jha et al. (CfA)	7011
1998ec.....	UGC 3576	1998 Sep 26.8	Y. Qiu et al. (BAO)	7022	S. Jha et al. (CfA)	7024
1998ef.....	UGC 646	1998 Oct 18.3	W. Li et al. (LOSS)	7032	A. Filippenko	7032
1998eg.....	UGC 12133	1998 Oct 19.9	T. Boles (UK)	7033	M. Salvo et al., S. Jha et al. (CfA)	7037
1998es.....	NGC 632	1998 Nov 13.3	E. Halderson et al. (LOSS)	7050	S. Jha et al. (CfA)	7054
1999X.....	CGCG 180-22	1999 Jan 23.2	M. Schwartz (TO)	7105	P. Garnavich et al. (CfA)	7105
1999aa.....	NGC 2595	1999 Feb 11.0	R. Arbour (UK)	7108	A. Filippenko et al.	7108
1999ac.....	NGC 6063	1999 Feb 26.5	M. Modjaz et al. (LOSS)	7114	M. Phillips, A. Filippenko	7122
1999cc.....	NGC 6038	1999 May 8.3	M. Schwartz (TO)	7163	P. Garnavich et al. (CfA)	7169
1999cl.....	NGC 4501 (M88)	1999 May 29	M. Papenkova et al. (LOSS)	7185	P. Garnavich et al. (CfA)	7190
1999cw.....	MCG −01-02-001	1999 Jun 28.5	R. Johnson & W. Li (LOSS)	7211	L. Rizzi et al.	7216
1999dq.....	NGC 976	1999 Sep 2.5	W. Li (LOSS)	7247	S. Jha et al. (CfA)	7250
1999ef.....	UGC 607	1999 Oct 9	J. Mueller	7275	M. Kuchner & D. Branch	7275
1999ej.....	NGC 495	1999 Oct 18.3	A. Friedman et al. (LOSS)	7286	S. Jha et al. (CfA)	7298
1999ek.....	UGC 3329	1999 Oct 20.5	R. Johnson & W. Li (LOSS)	7286	L. Strolger et al., S. Jha et al. (CfA)	7300
1999gd.....	NGC 2623	1999 Nov 24.5	W. Li (LOSS)	7319	A. Filippenko & P. Garnavich	7328
1999gh.....	NGC 2986	1999 Dec 3.8	K. Takamizawa	7328	A. Filippenko & P. Garnavich	7328
1999gp.....	UGC 1993	1999 Dec 23.2	M. Papenkova & W. Li (LOSS)	7337	S. Jha et al. (CfA)	7341
2000B.....	NGC 2320	2000 Jan 11.0	P. Antonini et al.	7347	F. Colas et al.	7351
2000ce.....	UGC 4195	2000 May 8.1	T. Puckett (POSS)	7417	S. Jha et al. (CfA)	7422
2000cf.....	MCG +11-19-25	2000 May 9.2	T. Puckett & A. Sehgal (POSS)	7421	S. Jha et al. (CfA)	7423
2000cn.....	UGC 11064	2000 Jun 2.5	M. Papenkova & W. Li (LOSS)	7436	S. Jha et al. (CfA), M. Turatto et al.	7437
2000cx.....	NGC 524	2000 Jul 17.5	C. Yu et al. (LOSS)	7458	R. Chornock et al.	7463
2000dk.....	NGC 382	2000 Sep 18.3	S. Beckmann & W. Li (LOSS)	7493	S. Jha et al. (CfA)	7494
2000fa	UGC 3770	2000 Nov 30.5	A. Friedman & W. Li (LOSS)	7533	T. Matheson et al. (CfA)	7535

used galaxy subtraction to perform the differential photometry of all the SNe Ia except for SN 2000cx, which was located very far from the nucleus of its (elliptical) host galaxy, where the galaxy background was negligible and template subtraction only added undesirable correlated noise. For SN 2000cx we performed point-spread function (PSF) fitting photometry on the SN and comparison stars using the DAOPHOT ALLSTAR (Stetson 1987, 1994) package in IRAF.

For the other 43 objects we employed template subtraction as follows: Generally, a number of late-time images were taken in each passband with exposure times comparable to or slightly longer than the deepest images with the SN present, and we chose the set of images with the best seeing to serve as the templates. For each passband, all the images were registered to the template, and the image subtraction was performed using the ISIS subtraction package (Alard & Lupton 1998) as modified by B. Schmidt (2001, private communication) to allow for more robust selection of regions in the two images suitable for determination of the convolution kernel (avoiding saturated stars, cosmic rays, and cosmetic defects). We subtracted the template from each SN image and replaced a small region around the SN with the template-subtracted version. In the typical case, in which the template image quality was better than the SN image, we convolved the template to the SN image, subtracted, and replaced the SN neighborhood from the subtracted image back into the original SN image. In the rare case in which the SN image quality was better than the template, we degraded the SN image to match the PSF of the template image, subtracted, and replaced the subtracted SN neighborhood back into the convolved (degraded) SN image. This procedure ensures that the PSF of the SN matches the PSF of the comparison stars. We also added artificial stars of known brightness into the SN images, mimicking the SN subtraction procedure on these stars. Finally, we performed aperture photometry, as well as DoPHOT PSF-fitting photometry (Schechter

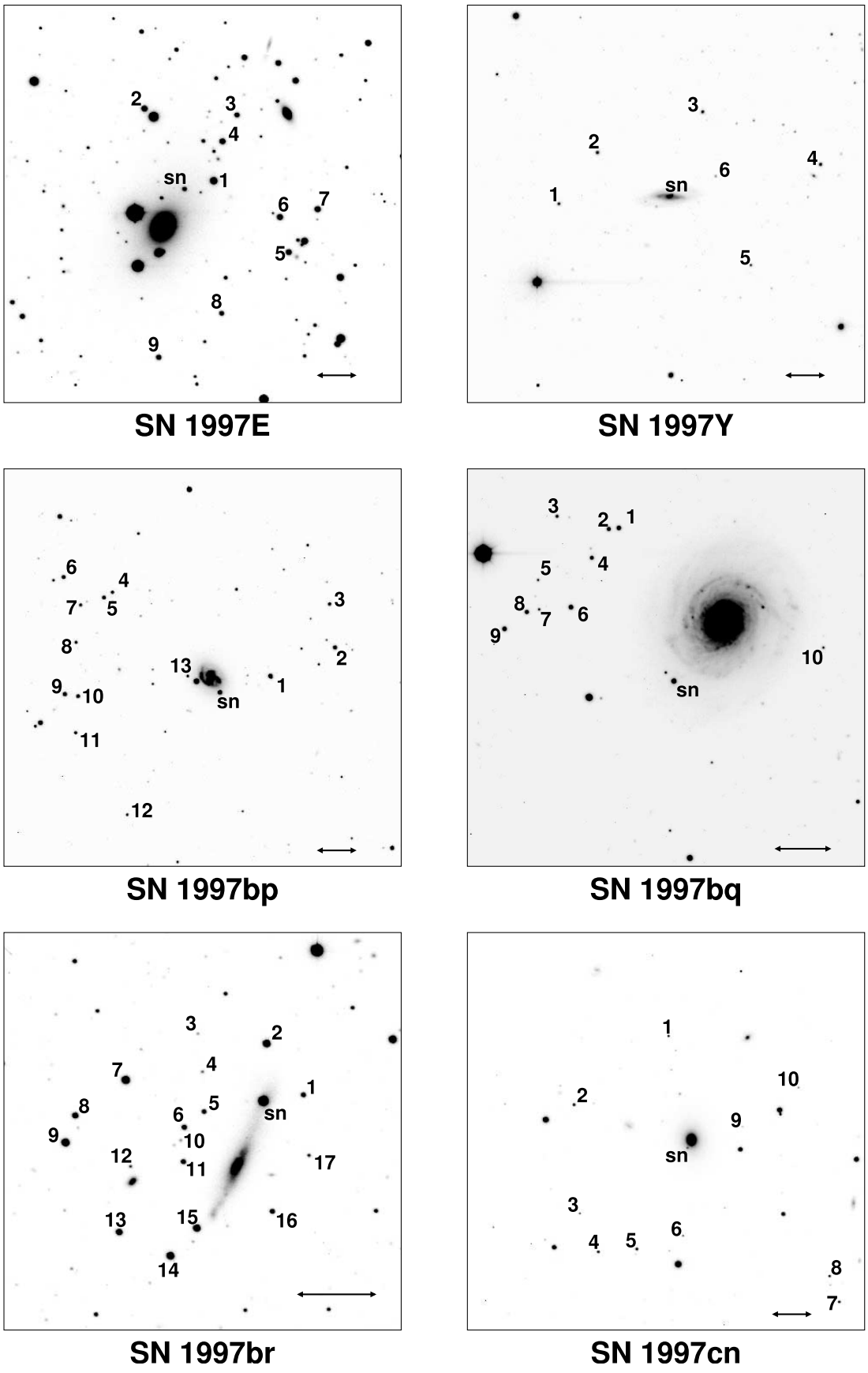

FIG. 1.—Finder charts for the 44 SNe Ia presented here and the associated comparison stars. The images are a combination of all the *R*-band SN images. North is up, and east is to the left. The horizontal double arrow in the lower right delineates 1′.

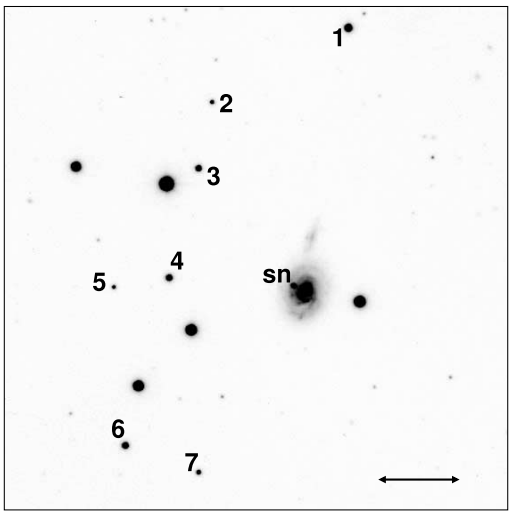

SN 1997cw

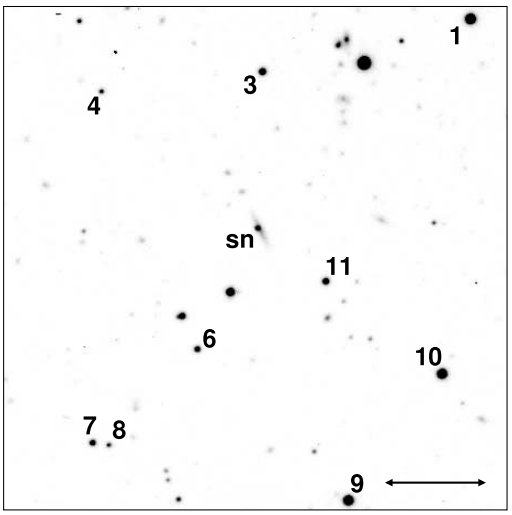

SN 1997dg

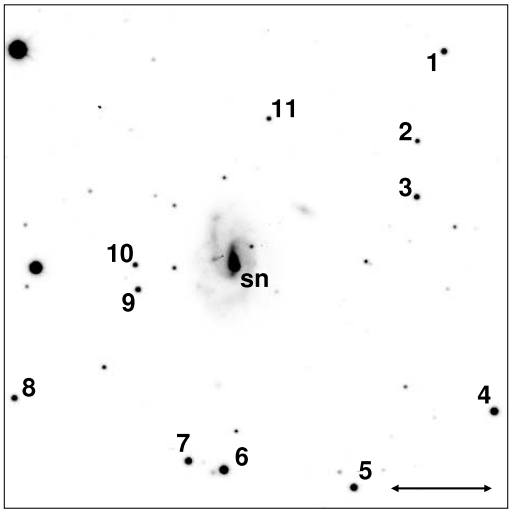

SN 1997do

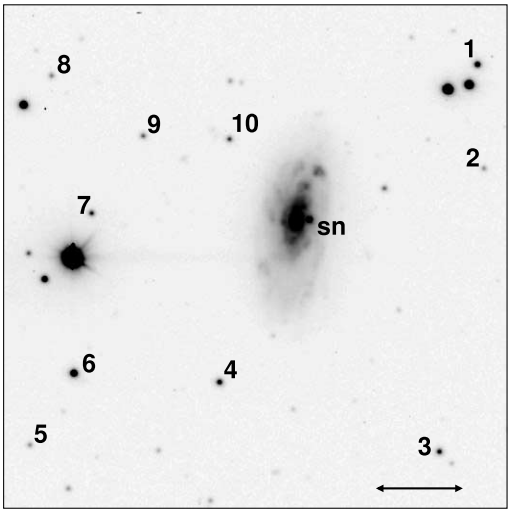

SN 1997dt

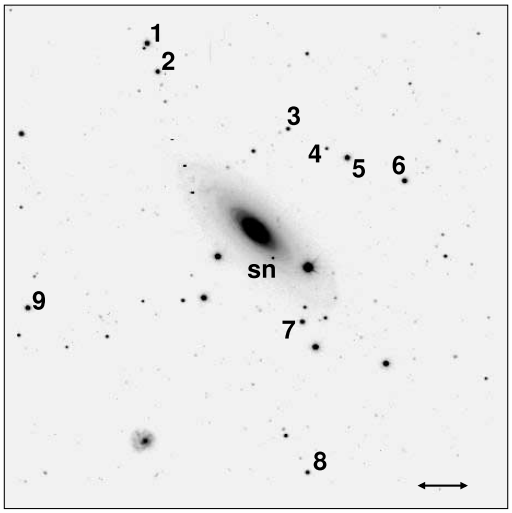

SN 1998D

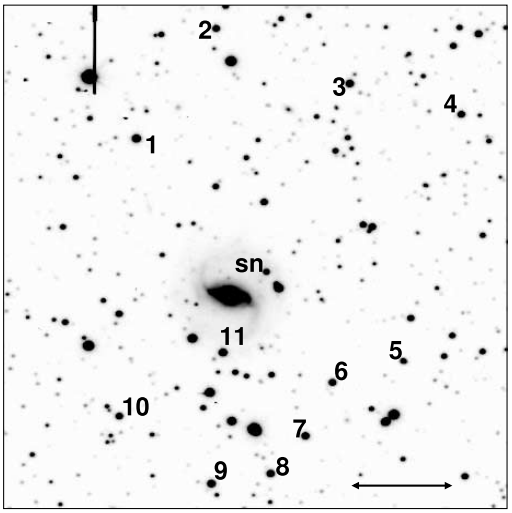

SN 1998V

FIG. 1.—*Continued*

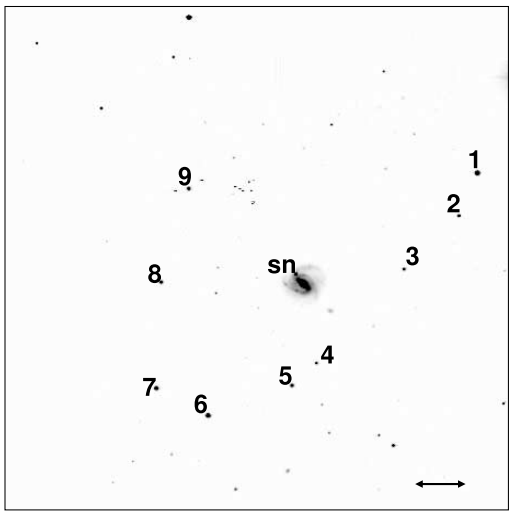

SN 1998ab

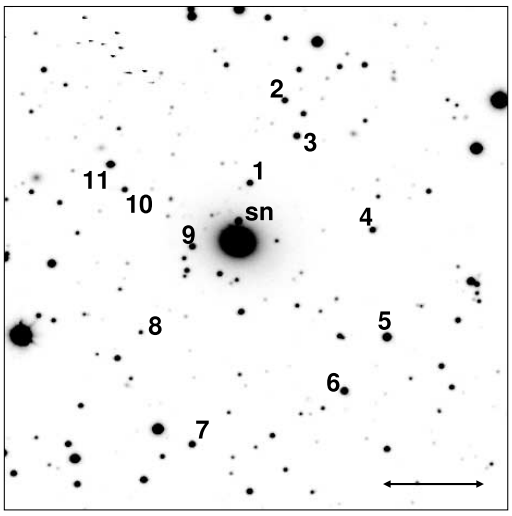

SN 1998bp

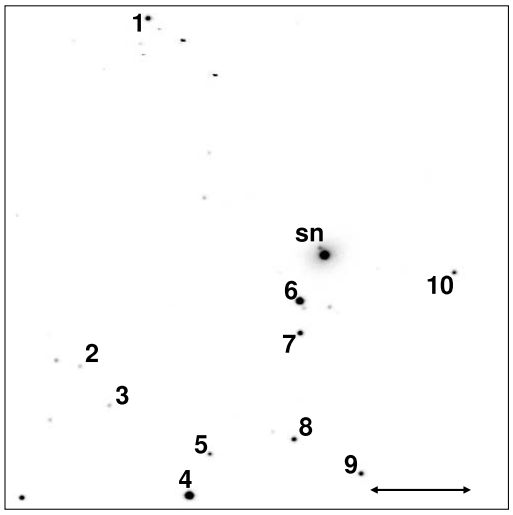

SN 1998co

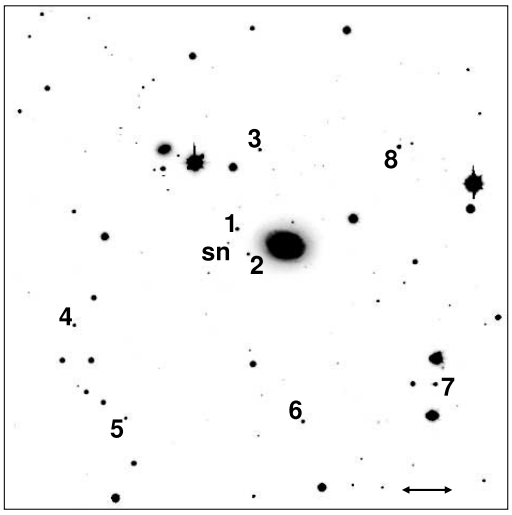

SN 1998de

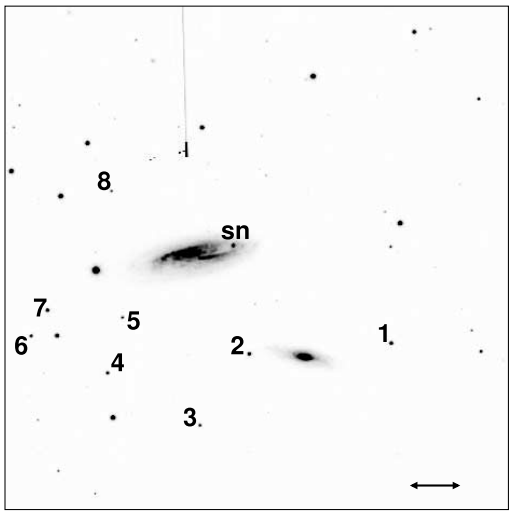

SN 1998dh

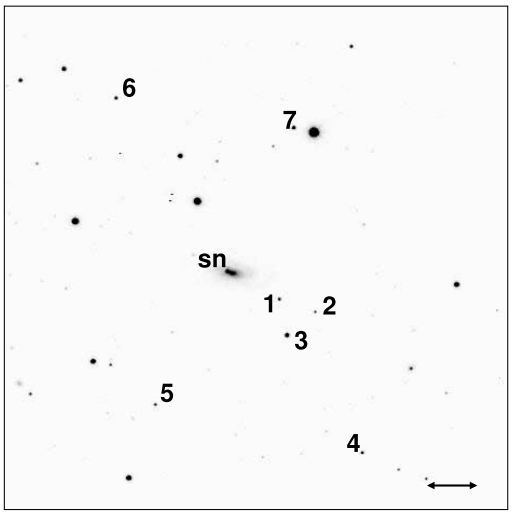

SN 1998dk

FIG. 1.—*Continued*

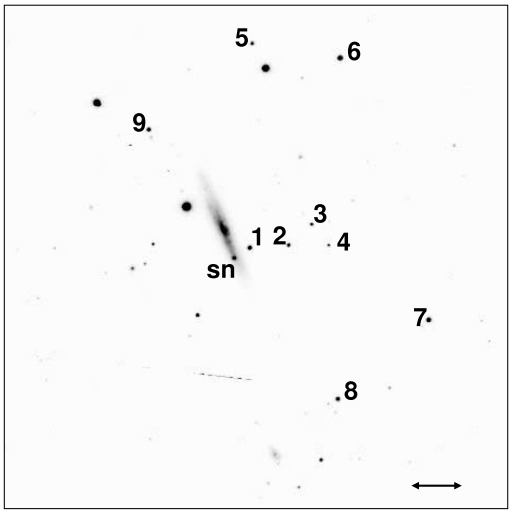

SN 1998dm

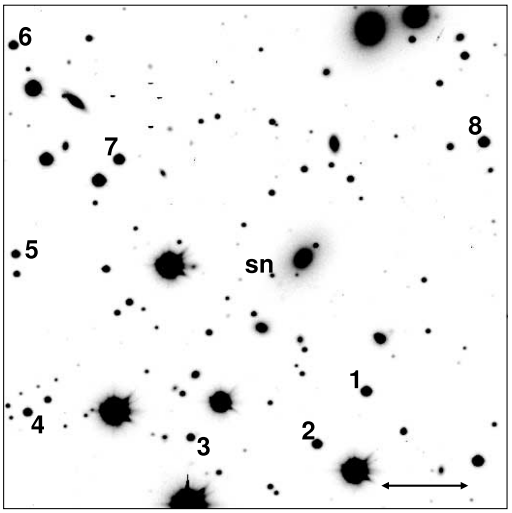

SN 1998dx

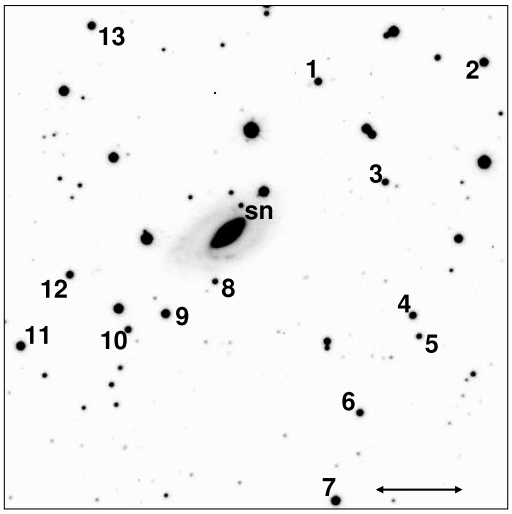

SN 1998ec

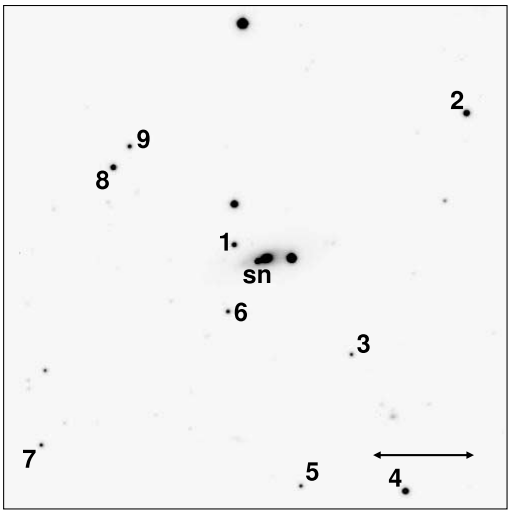

SN 1998ef

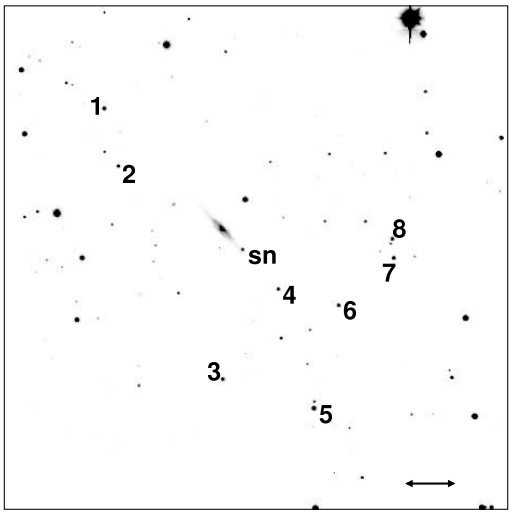

SN 1998eg

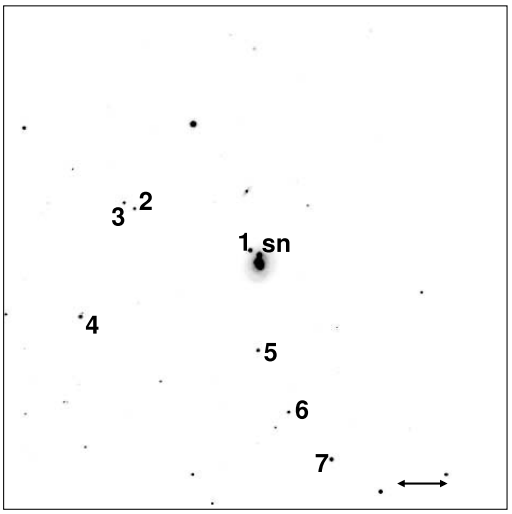

SN 1998es

FIG. 1.—*Continued*

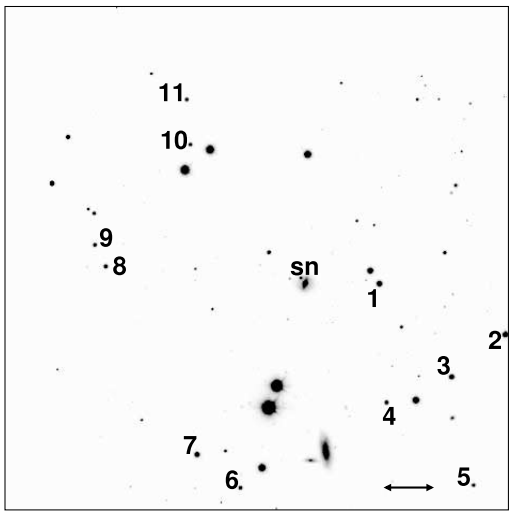

SN 1999X

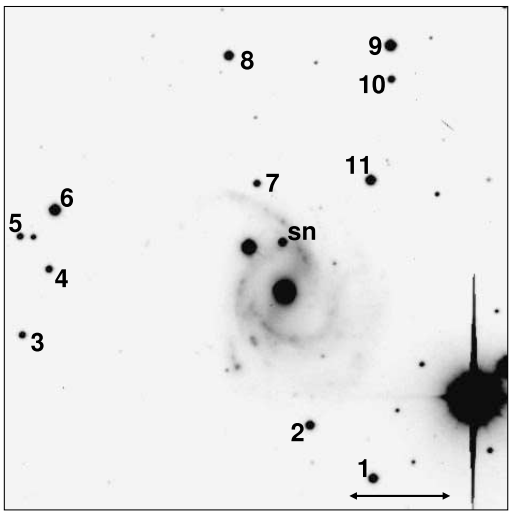

SN 1999aa

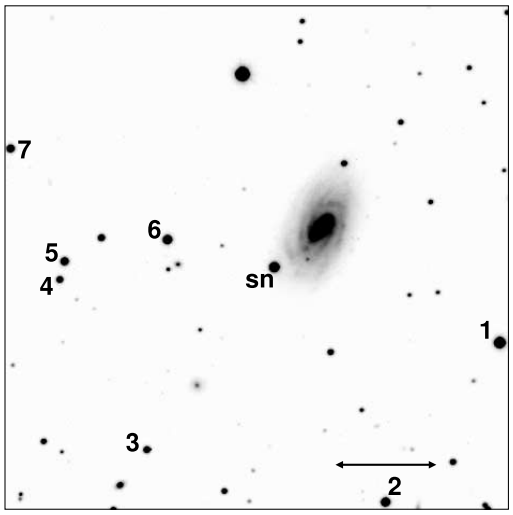

SN 1999ac

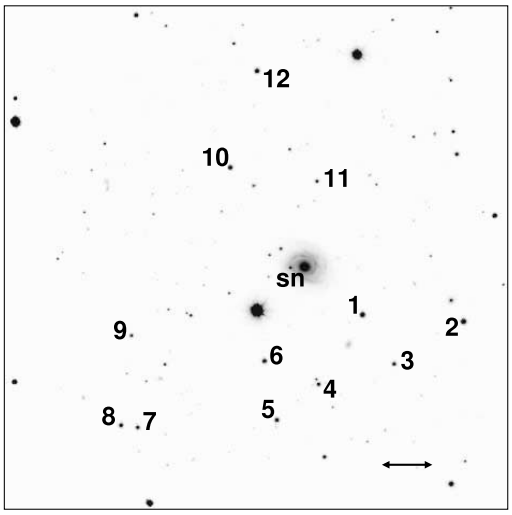

SN 1999cc

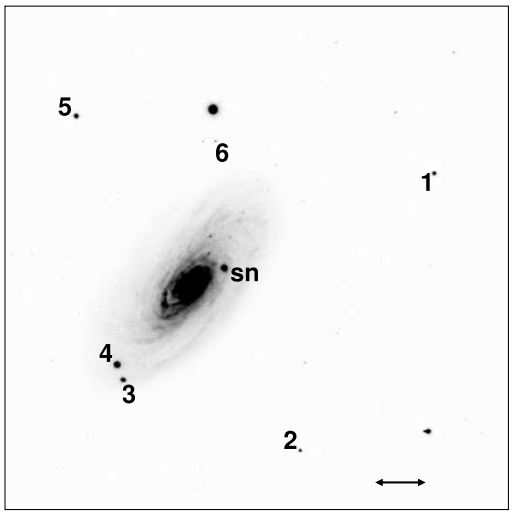

SN 1999cl

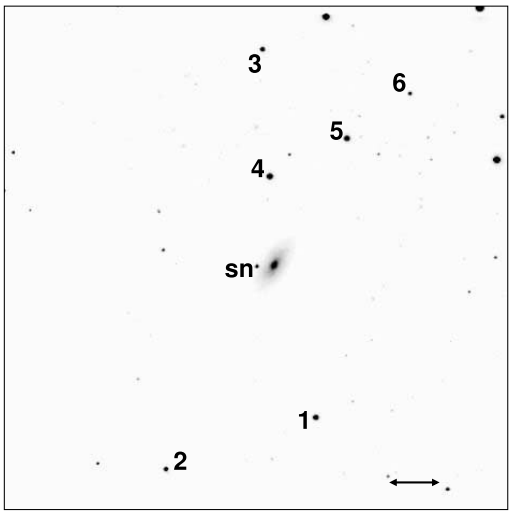

SN 1999cw

FIG. 1.—*Continued*

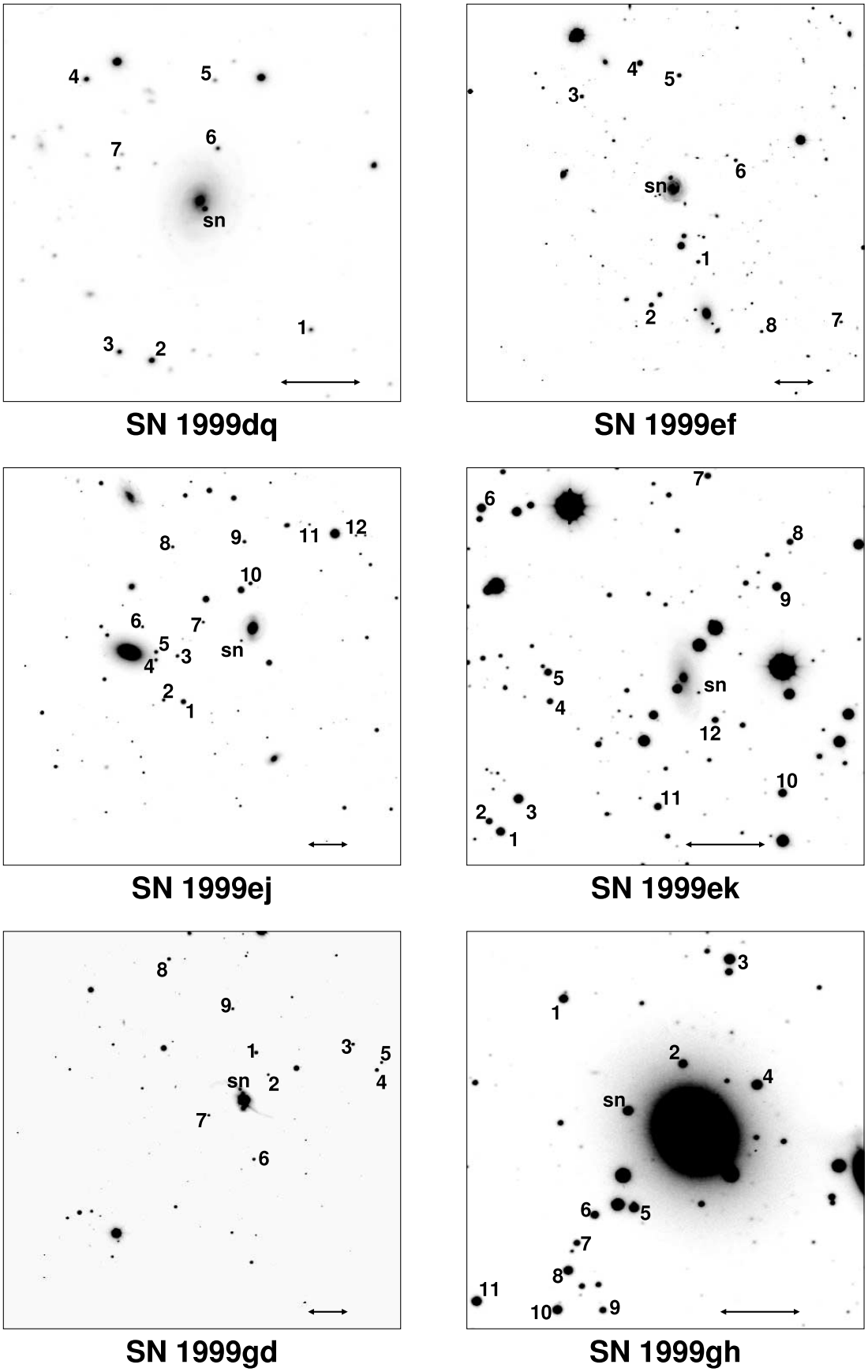

FIG. 1.—*Continued*

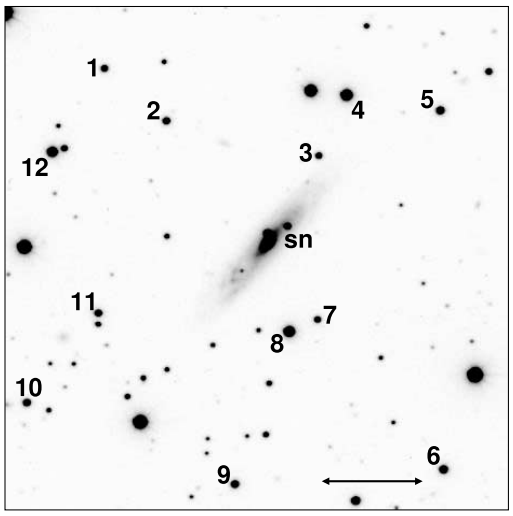

SN 1999gp

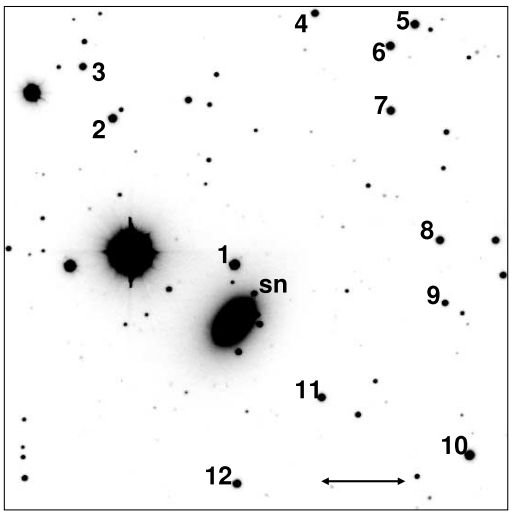

SN 2000B

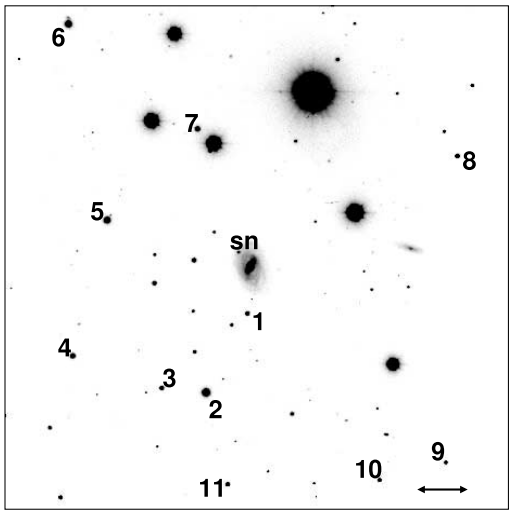

SN 2000ce

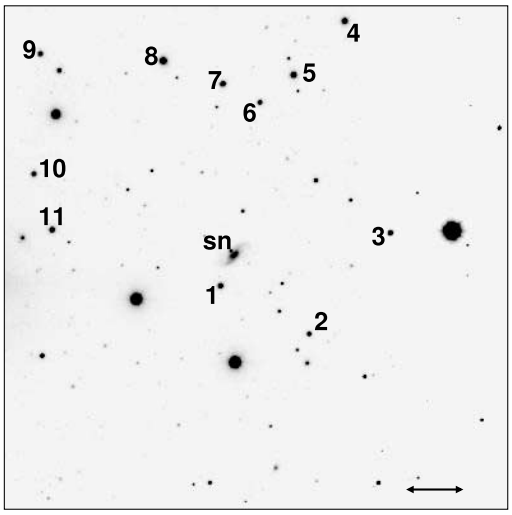

SN 2000cf

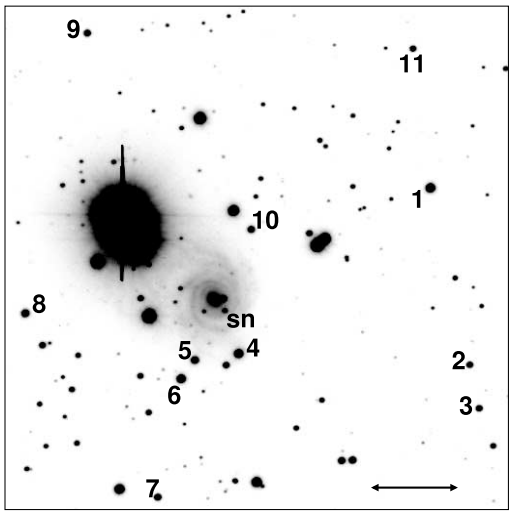

SN 2000cn

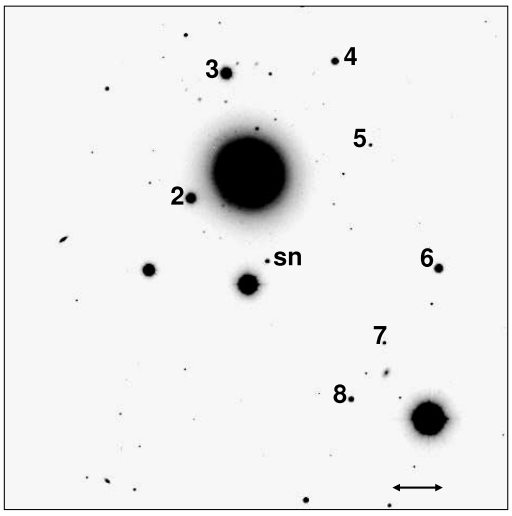

SN 2000cx

FIG. 1.—*Continued*

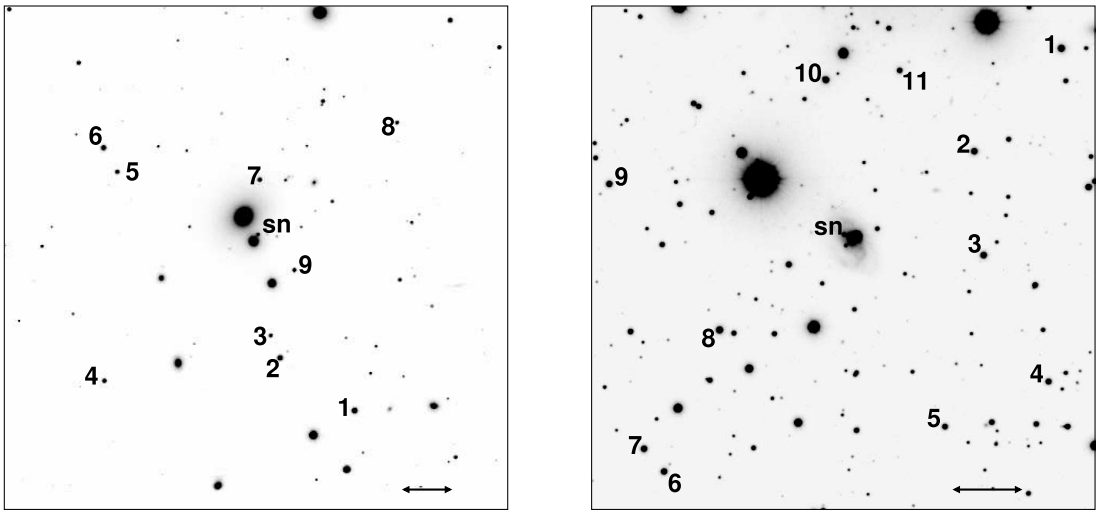

FIG. 1.—*Continued*

et al. 1993), on the SN, comparison stars, and artificial stars in the galaxy-subtracted images. We checked that the recovered magnitudes of the added stars matched their input magnitudes and that the aperture and PSF photometry gave consistent results, generally to better than 0.01 mag. We also verified that this photometry derived via galaxy subtraction was consistent with direct PSF photometry for SNe for which the galaxy background was exceptionally smooth. For our final differential photometry, we chose to use the aperture photometry of the SNe and comparison stars, with an aperture radius given by 0.75 times the FWHM of the PSF.

This general strategy is identical to that used by the High-Z Supernova Search Team (Schmidt et al. 1998) in analysis of high-redshift SNe Ia; while the actual software is in a state of constant evolution, we have used one incarnation for all the light curves presented here. The result of this process is homogeneous and reliable differential *UBVRI* photometry of each SN and its associated comparison stars in the natural system of the observations (i.e., instrumental magnitudes).

2.4. *Calibration*

We calibrate each of the SN fields following the precepts of Harris et al. (1981), using the all-sky *UBVRI* standard stars of Landolt (1992). On photometric nights, we typically observe on the order of 10–15 Landolt fields over a wide range of air mass (generally from 1.1 to ~2). We perform aperture photometry on the reduced Landolt fields using the APPHOT package in IRAF, using a 6 pixel aperture radius (~4″) that is then corrected to a 15 pixel radius (~10″) via a curve of growth defined by a few isolated, bright stars in each image. We then determine the zero points and transformation coefficients linear in air mass and color from the instrumental magnitudes *ubvri* to the standard Landolt *UBVRI* magnitudes and $U-B$, $B-V$, $V-R$, and $V-I$ colors. For nights when many standard stars were observed, we check the linear solution by also fitting a quadratic term in color, as well as a color times air-mass term; in all cases the coefficients for the higher order terms are negligible, and so we use only the linear solutions. Because of the different detector and filter set combinations we have used, we take care to keep track of the transformation coefficients separately. As expected, for a given detector–filter set combination, the variations in the zero points and air-mass terms are small but significant, while the color terms are always consistent within the fit uncertainties.

Once we have the standard solution for a photometric night, we apply this solution to the instrumental aperture magnitudes of the comparison stars in each SN field, measured in exactly the same way as the Landolt standard stars. This yields the standard *UBVRI* magnitudes of the comparison stars in each SN field. For most of the fields, we have several calibrations, enabling us to average the results and identify and eliminate outliers. For a handful of SNe, however, we have only one night of photometric calibration, a somewhat perilous situation. Nevertheless, for every one of these objects we have checked that other SN fields taken on the same night have photometry that is consistent on other nights, bolstering our confidence that the photometry of objects with only one night of calibration is not significantly in error. In Table 2 we present the final comparison star V magnitudes and colors with their uncertainties (in the mean), as well as the number of photometric nights averaged to yield the results. We also give positions of the SNe and comparison stars referenced to the USNO-A2.0 catalog (Monet et al. 1998), with a typical rms uncertainty of ±0.″3. The locations of the SNe and comparison stars are shown in Figure 1.

We present the average color terms for each detector–filter set combination in Table 3, along with the internal uncertainties in the mean. We do not have data on any photometric nights when the AndyCam and the Harris filters were on the telescope, and thus, we could not use observations of standard stars to determine the color terms for this detector–filter set combination. Instead, we used the color terms based on the calibrated comparison stars themselves (allowing for a variable zero point for each frame, given the nonphotometric conditions). For the other detector–filter set combinations, we successfully used this method to check the color terms for consistency.

Armed with the comparison star standard magnitudes and the color terms for each detector–filter set combination, we determined the zero point for each SN image by transforming the comparison star standard magnitudes to instrumental magnitudes (using the appropriate color term) and comparing them to the observed comparison star magnitudes. Because the SN is observed at the same time (and thus, air mass) as the comparison

TABLE 2
COMPARISON STAR PHOTOMETRY

Star	α (J2000.0)	δ (J2000.0)	V	$U-B$	$B-V$	$V-R$	$V-I$	N
				SN 1997E				
SN	06 47 38.16	+74 29 51.0						
1.....	06 47 27.41	+74 30 02.6	14.402 ± 0.014	0.086 ± 0.041	0.675 ± 0.011	0.427 ± 0.007	0.846 ± 0.010	3
2.....	06 47 52.40	+74 31 52.6	15.139 ± 0.015	0.123 ± 0.040	0.715 ± 0.011	0.436 ± 0.007	0.863 ± 0.010	3
3.....	06 47 18.41	+74 31 40.7	15.895 ± 0.017	0.018 ± 0.040	0.584 ± 0.013	0.365 ± 0.008	0.747 ± 0.009	3
4.....	06 47 23.92	+74 31 01.6	15.410 ± 0.022	0.580 ± 0.045	0.946 ± 0.019	0.539 ± 0.007	1.021 ± 0.014	3
5.....	06 47 00.39	+74 28 13.5	15.358 ± 0.014	0.594 ± 0.041	0.907 ± 0.012	0.511 ± 0.009	0.968 ± 0.009	3
6.....	06 47 03.36	+74 29 06.4	15.152 ± 0.013	0.143 ± 0.040	0.733 ± 0.012	0.439 ± 0.008	0.877 ± 0.010	3
7.....	06 46 49.48	+74 29 17.2	15.181 ± 0.014	0.390 ± 0.042	0.833 ± 0.012	0.481 ± 0.009	0.930 ± 0.013	3
8.....	06 47 25.35	+74 26 43.6	16.150 ± 0.015	0.231 ± 0.045	0.812 ± 0.011	0.476 ± 0.009	0.926 ± 0.012	3
9.....	06 47 48.60	+74 25 39.1	15.718 ± 0.014	0.055 ± 0.040	0.657 ± 0.011	0.399 ± 0.007	0.800 ± 0.009	3

NOTES.—Units of right ascension are hours, minutes, and seconds, and units of declination are degrees, arcminutes, and arcseconds. Table 2 is published in its entirety in the electronic edition of the *Astronomical Journal*. A portion is shown here for guidance regarding its form and content.

stars, the air-mass term is absorbed into the zero point, which is robustly determined from the flux-weighted average of the comparison stars. We then use this zero point to determine calibrated instrumental magnitudes for the SN and use the linear color term transformation to arrive at the final Landolt standard magnitudes for the SN. We keep track of and propagate the uncertainties throughout this procedure, including photon noise in the instrumental magnitudes, dispersion in the photometric solution, uncertainties in the transformation coefficients, and internal uncertainty in the zero point for each image. The final standard system *UBVRI* magnitudes of the SNe, along with the uncertainties and the detector–filter set combination, are given in Table 4. The *UBVRI* light curves of the 44 SNe Ia are shown in Figure 2 relative to maximum light (defined in the *B* band) and corrected for time dilation to the SN rest frame (see Table 6, § 3.2).

TABLE 3
PHOTOMETRIC COLOR TERMS

Detector/Filter Set	Color Term	Value	Nights
AndyCam/SAO	$(v-V)/(B-V)$	+0.0340 ± 0.0042	7
	$(u-b)/(U-B)$	0.9312 ± 0.0039	6
	$(b-v)/(B-V)$	0.9293 ± 0.0029	7
	$(v-r)/(V-R)$	0.9824 ± 0.0053	7
	$(v-i)/(V-I)$	1.0739 ± 0.0040	7
AndyCam/Harris + I_{SAO}[a]	$(v-i)/(V-I)$	1.0639 ± 0.0124	2[b]
AndyCam/Harris	$(v-V)/(B-V)$	+0.0441 ± 0.0061	3[b]
	$(u-b)/(U-B)$	0.9617 ± 0.0130	3[b]
	$(b-v)/(B-V)$	0.9631 ± 0.0149	3[b]
	$(v-r)/(V-R)$	1.0947 ± 0.0203	3[b]
	$(v-i)/(V-I)$	0.9899 ± 0.0224	1[b]
4Shooter, chip 1/SAO	$(v-V)/(B-V)$	+0.0423 ± 0.0043	3
	$(u-b)/(U-B)$	0.9433 ± 0.0111	3
	$(b-v)/(B-V)$	0.8937 ± 0.0171	3
	$(v-r)/(V-R)$	0.9873 ± 0.0126	3
	$(v-i)/(V-I)$	1.0837 ± 0.0206	3
4Shooter, chip 3/SAO	$(v-V)/(B-V)$	+0.0398 ± 0.0052	4
	$(u-b)/(U-B)$	0.9650 ± 0.0156	1
	$(b-v)/(B-V)$	0.8830 ± 0.0100	4
	$(v-r)/(V-R)$	0.9685 ± 0.0190	2
	$(v-i)/(V-I)$	1.0725 ± 0.0024	4
4Shooter, chip 3/Harris + I_{SAO}[a]	$(v-i)/(V-I)$	1.0900 ± 0.0149	1
4Shooter, chip 3/Harris	$(v-V)/(B-V)$	0.0447 ± 0.0009	19
	$(u-b)/(U-B)$	0.9638 ± 0.0081	18
	$(b-v)/(B-V)$	0.9155 ± 0.0035	19
	$(v-r)/(V-R)$	1.0812 ± 0.0026	19
	$(v-i)/(V-I)$	1.0284 ± 0.0016	17

NOTES.—The lowercase and uppercase letters in the color terms refer to instrumental and standard magnitudes, respectively. All color terms implicitly contain an additive constant. For example, for the AndyCam/SAO combination, $(v-V) = +0.0340(B-V) + \text{const}$ and $(u-b) = 0.9312(U-B) + \text{const}$.

[a] This filter set consists of the Harris *UBVR* filters and the SAO *I* filter.

[b] These nights were not photometric; the color terms were derived from the calibrated comparison stars. See text for details.

TABLE 4
SUPERNOVA PHOTOMETRY

HJD	*U*	*B*	*V*	*R*	*I*	Detector/Filter Set
			SN 1997E			
2,450,464.92.....	...	15.694 0.017	15.598 0.011	15.377 0.015	...	AndyCam/SAO
2,450,465.69.....	15.441 0.038	15.667 0.015	15.544 0.010	15.357 0.013	15.423 0.014	AndyCam/SAO
2,450,466.78.....	15.414 0.036	15.656 0.013	15.502 0.008	15.323 0.011	15.468 0.011	AndyCam/SAO
2,450,468.66.....	15.500 0.037	15.620 0.014	15.492 0.010	15.322 0.012	15.480 0.013	AndyCam/SAO
2,450,472.66.....	15.789 0.037	15.779 0.013	15.491 0.008	15.323 0.013	15.638 0.012	AndyCam/SAO
2,450,476.89.....	16.330 0.061	16.166 0.032	15.741 0.023	15.716 0.030	15.940 0.032	AndyCam/SAO
2,450,479.87.....	16.802 0.037	16.547 0.013	15.933 0.008	15.906 0.011	16.006 0.011	AndyCam/SAO
2,450,485.62.....	17.725 0.041	17.381 0.015	16.301 0.009	16.003 0.013	15.847 0.018	AndyCam/SAO
2,450,489.77.....	...	17.891 0.022	16.627 0.014	16.131 0.019	15.823 0.019	AndyCam/SAO
2,450,512.65.....	19.247 0.060	18.929 0.025	17.829 0.016	17.448 0.026	17.296 0.023	AndyCam/SAO

NOTES.—Table 4 is published in its entirety in the electronic edition of the *Astronomical Journal*. A portion is shown here for guidance regarding its form and content.

We have used linear color transformations between the SN instrumental magnitudes and standard magnitudes as has been conventional when presenting SN Ia light curves, but these may be inappropriate due to the strong, broad features present in SN spectra, as compared to the stars from which the color terms are derived. Fortunately, our primary concern is accurate photometry of SNe Ia near and soon after maximum light, when the SN flux is still dominated by the continuum in this "photospheric" phase, in which the linear transformations derived from stars would be most appropriate. Furthermore, for most of the detector–filter set combinations, the color terms do not strongly suggest the effective wavelengths are far from the standard bandpasses. The ultimate test, however, is in the light curves, which also give no evidence for systematic differences between observations taken with different detector–filter set combinations. For instance, the smoothness of the light curve of SN 1998es, observed with both instruments with multiple filter sets, is evidence of the internal consistency and homogeneity of the photometry. This is particularly important in the *U* band, for which this sample represents the first large collection of SN Ia photometry but which is also notoriously difficult to transform to a standard system (see, e.g., Suntzeff et al. 1999; Jha et al. 1999).

Although we have strived to ensure that the transformations to the standard system result in consistent, homogeneous photometry, the future uses of these data might nonetheless be limited by the accuracy of these transformations. It may be more convenient and useful to have the data as measured in the natural system. Given the color terms in Table 3, it is straightforward to transform the data back to the natural system (the natural system magnitudes are available on request). This is only useful, however, in conjunction with the natural system passbands. We have synthesized these passbands by combining the primary and secondary mirror reflectivities (taken simply as two reflections off an aluminum surface), the measured filter transmissions, and the measured detector QEs.[3] We have assumed that the shape of the QE curves for the two 4Shooter chips is identical. The synthesized passbands are shown in Figure 3, along with the standard *UX* and *BVRI* passbands of Bessell (1990). Because the *U* passband is defined by the atmospheric cutoff in the blue, we follow the Bessell convention of realizing this passband at air mass 1.0 (using the IRAF Kitt Peak atmospheric extinction curve, adjusted to match the average observed extinction coefficients), whereas the *BVRI* passbands are extra-atmospheric (i.e., air mass 0). As shown in Figure 3, the correspondence between the natural system passbands and the Bessell standard response curves is quite good, save for the *I* band in the SAO filter set. The synthesized passbands are also given in Table 5.

Through synthetic photometry we have verified that the natural system passbands yield color terms consistent with those directly measured (Table 3). We have also tried to constrain the natural system passbands directly, through observations of spectrophotometric standard stars on the photometric night of 2001 October 24 UT with the FLWO 1.2 m telescope using chip 3 of the 4Shooter and the Harris filter set. We took multiple *UBVRI* observations of the following eight tertiary spectrophotometric standard stars (Massey et al. 1988; Hamuy et al. 1992) over a wide air mass range throughout the night: BD +28 4211, Feige 34, Feige 110, G191B2B, Hiltner 600, LTT 9239, LTT 9491, and Wolf 1346. All these stars also have published spectrophotometry in the red to 1 μm (Massey & Gronwall 1990; Hamuy et al. 1994), allowing us to measure synthetic *BVRI* magnitudes. The ground-based spectrophotometry does not extend far enough to the blue with enough precision to synthesize *U* magnitudes (the Bessell *UX* passband extends down to 300 nm), and so for the *U* band we have used the results of Bohlin et al. (2001), who give *Hubble Space Telescope* STIS fluxes for five of the standards (BD +28 4211, Feige 34, Feige 110, G191B2B, and LTT 9491) extending below the atmospheric limit.

For each passband we model the response curve as a cubic spline through a number of spline points spaced equally over the wavelength region where we expect a nonzero response. For each observation in the passband ($\sim$20 each in *BVRI* and 13 in *U*), we correct the standard star spectrum for atmospheric extinction (as above, to 0 air mass for *BVRI* and 1.0 air mass for *U*) and synthesize photometry using the model passband. We find the best-fit model passband by minimizing the residuals between the synthetic and observed magnitudes, using a downhill-simplex (amoeba) method (Press et al. 1992). Our model is specified by the amplitudes (restricted to between 0 and 1) at the fixed spline points, with the normalization adjusted to yield a fixed zero point. The number of spline points in our model is somewhat arbitrary, limited by the number of individual measurements ($\sim$20 in *BVRI* and 13 in *U*). We have found that, in general, having fewer spline points is generally advantageous,

[3] We reiterate the footnote of Suntzeff et al. (1999) that the Bessell (1990) passband convention that we adopt also includes a term in the passband that is a linearly increasing function of wavelength. In this convention, then, the magnitude measured with a photon-counting detector is $m = -2.5 \log\left[\int F_\lambda(\lambda) R(\lambda)\, d\lambda\right] + \text{const}$, where $F_\lambda(\lambda)$ is the source flux density and $R(\lambda)$ is the bandpass response.

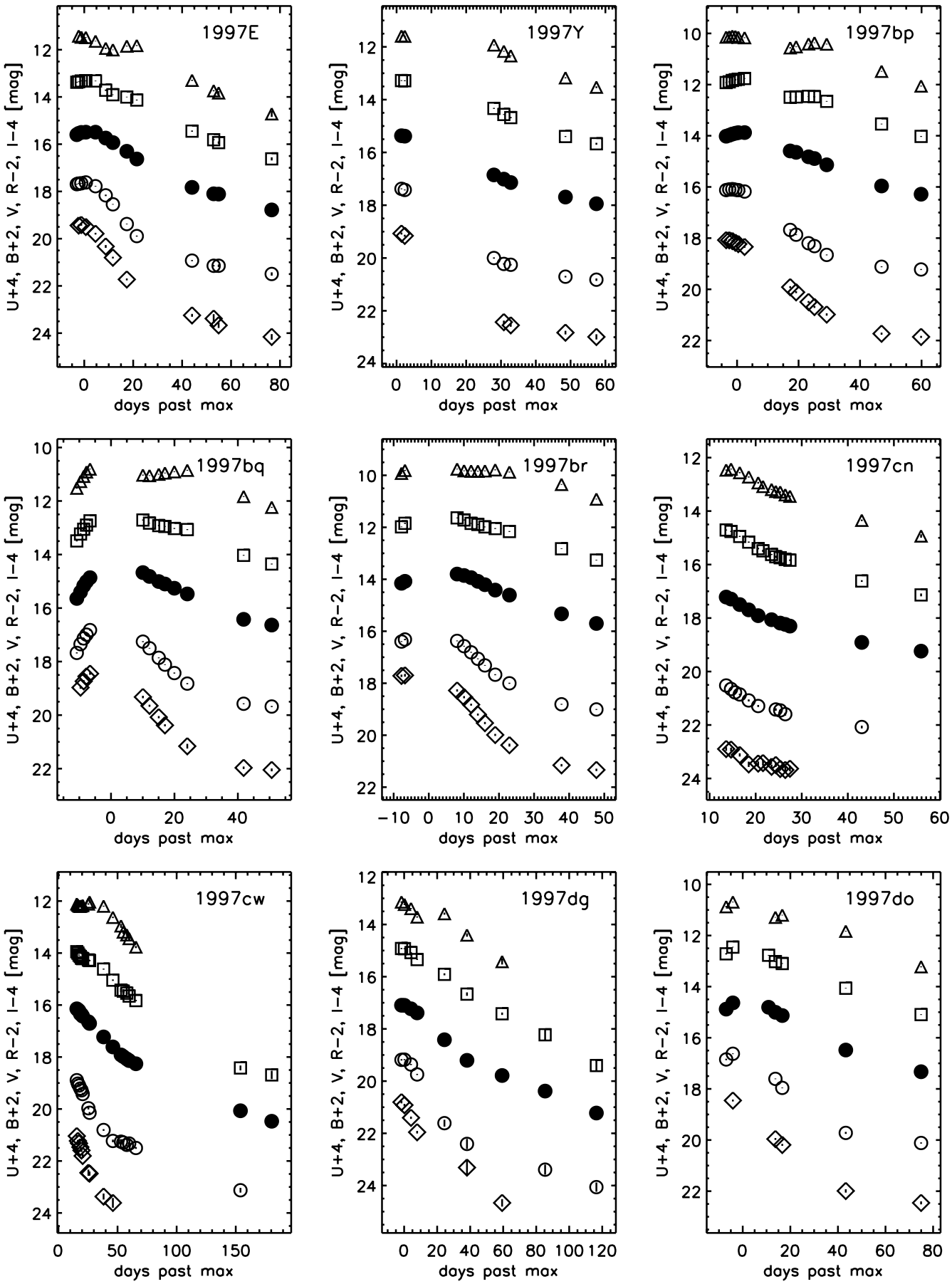

FIG. 2.—*UBVRI* photometry of 44 SNe Ia. The *U* (*diamonds*), *B* (*open circles*), *V* (*filled circles*), *R* (*squares*), and *I* (*triangles*) light curves are shown relative to *B* maximum and have been corrected for time dilation to the SN rest frame.

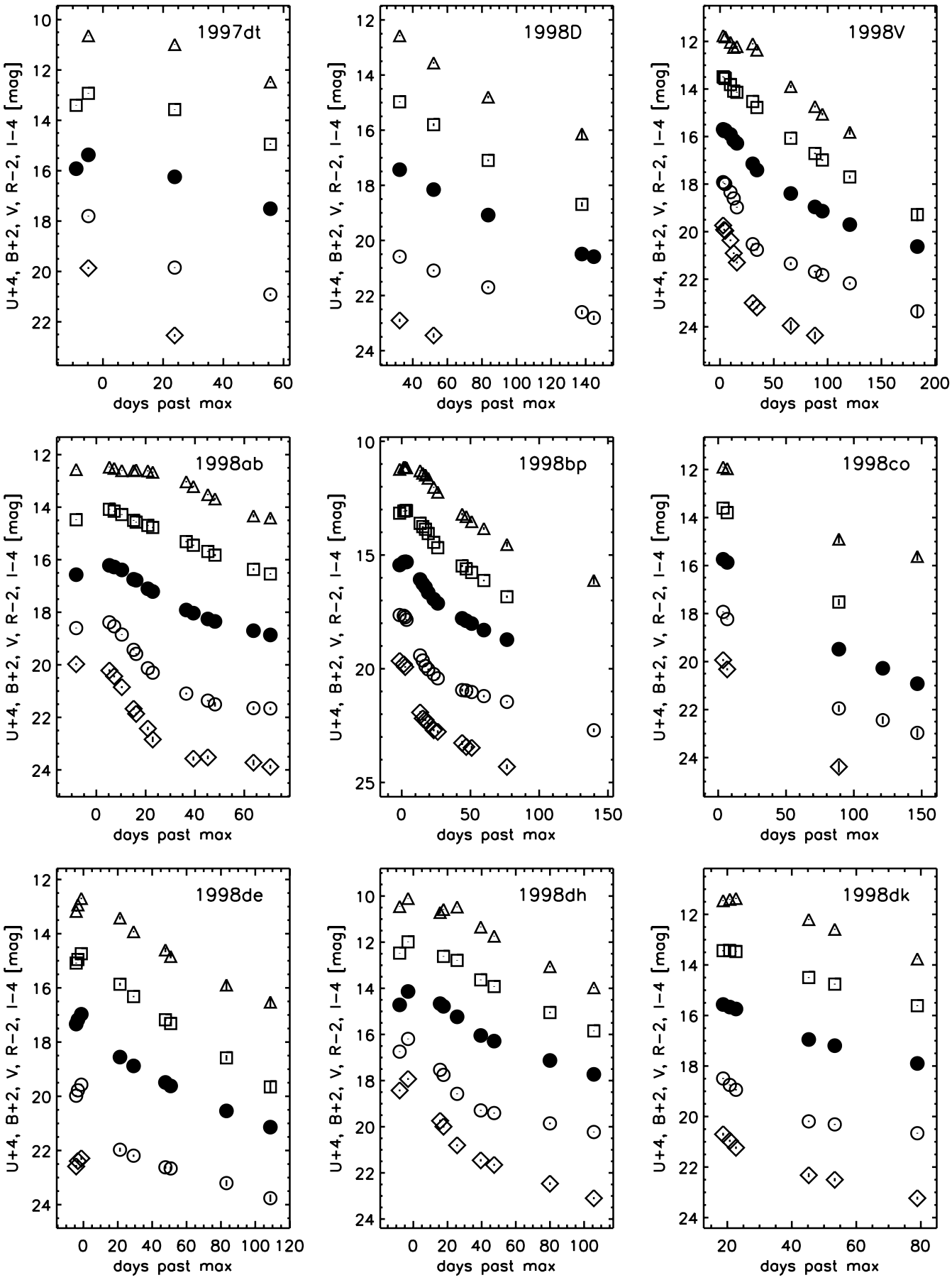

FIG. 2.—*Continued*

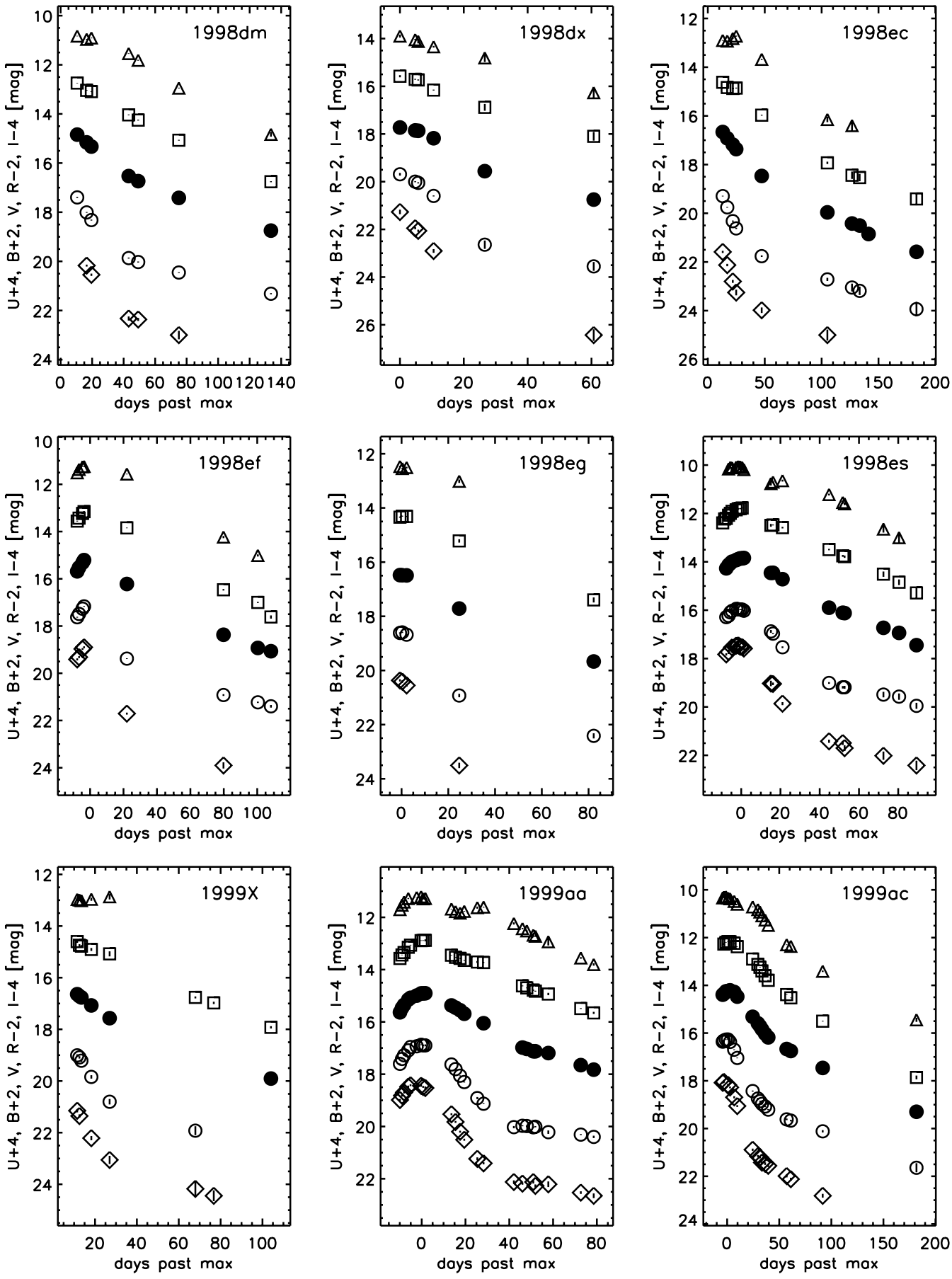

FIG. 2.—*Continued*

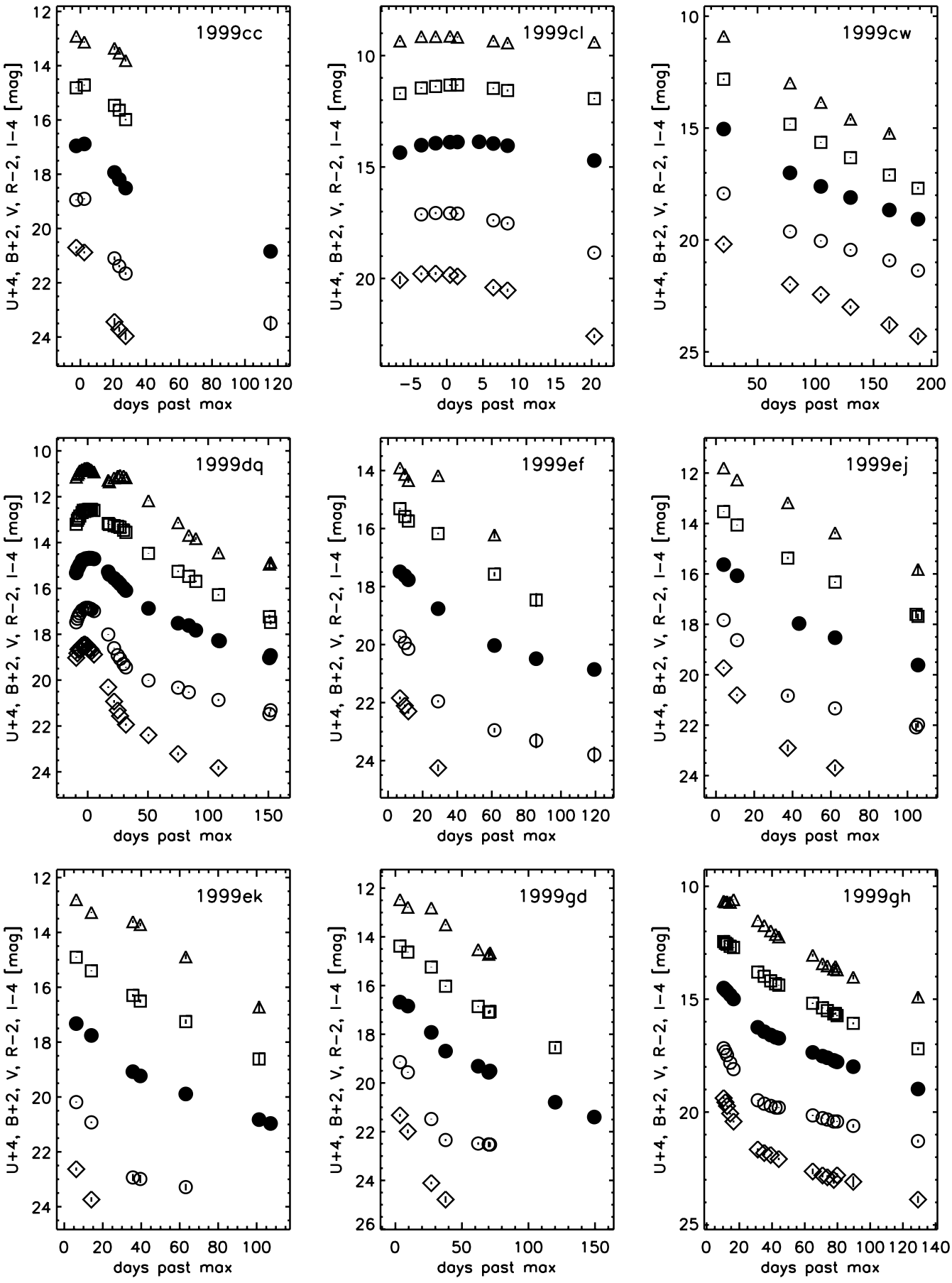

FIG. 2.—*Continued*

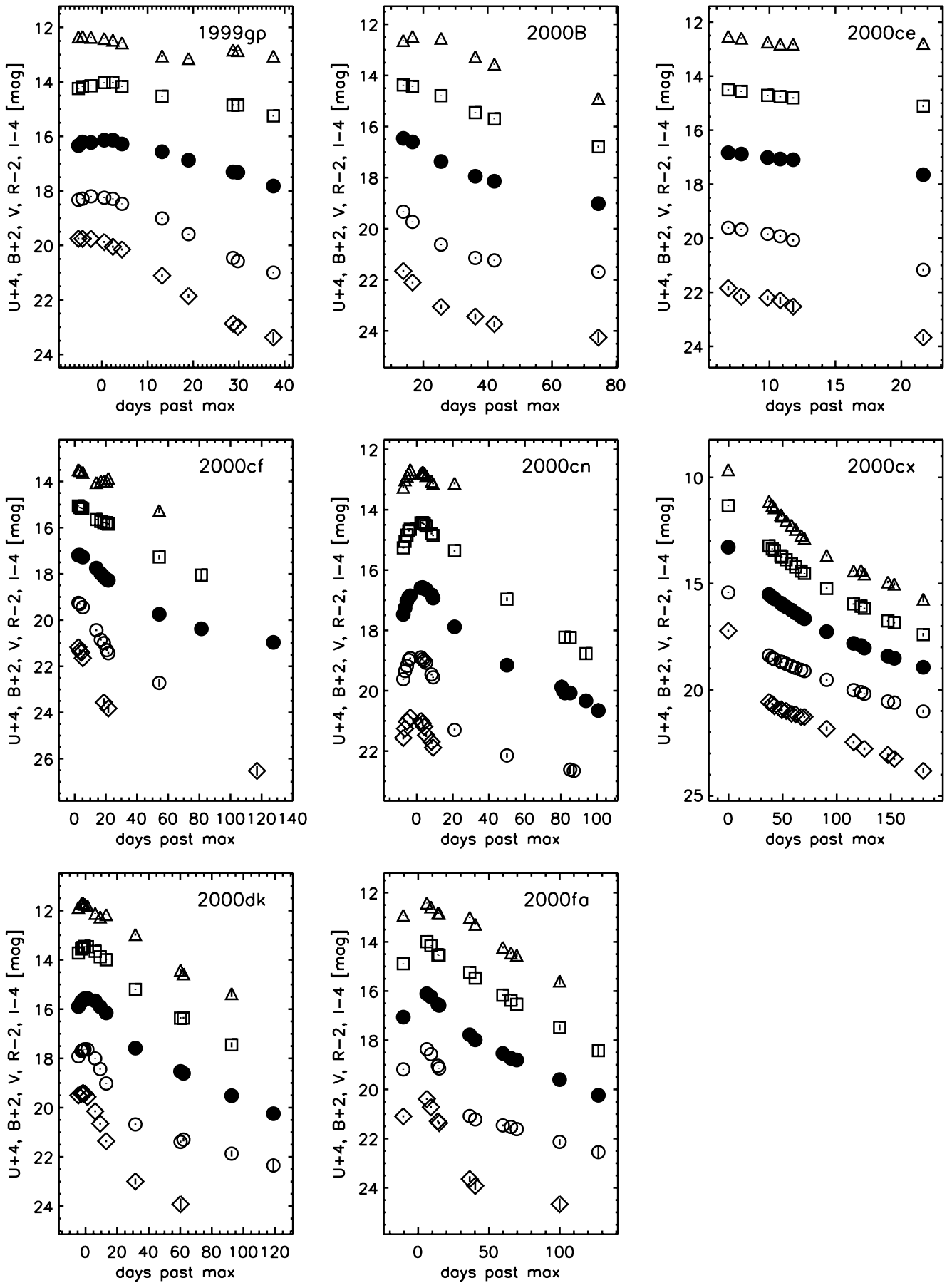

FIG. 2.—*Continued*

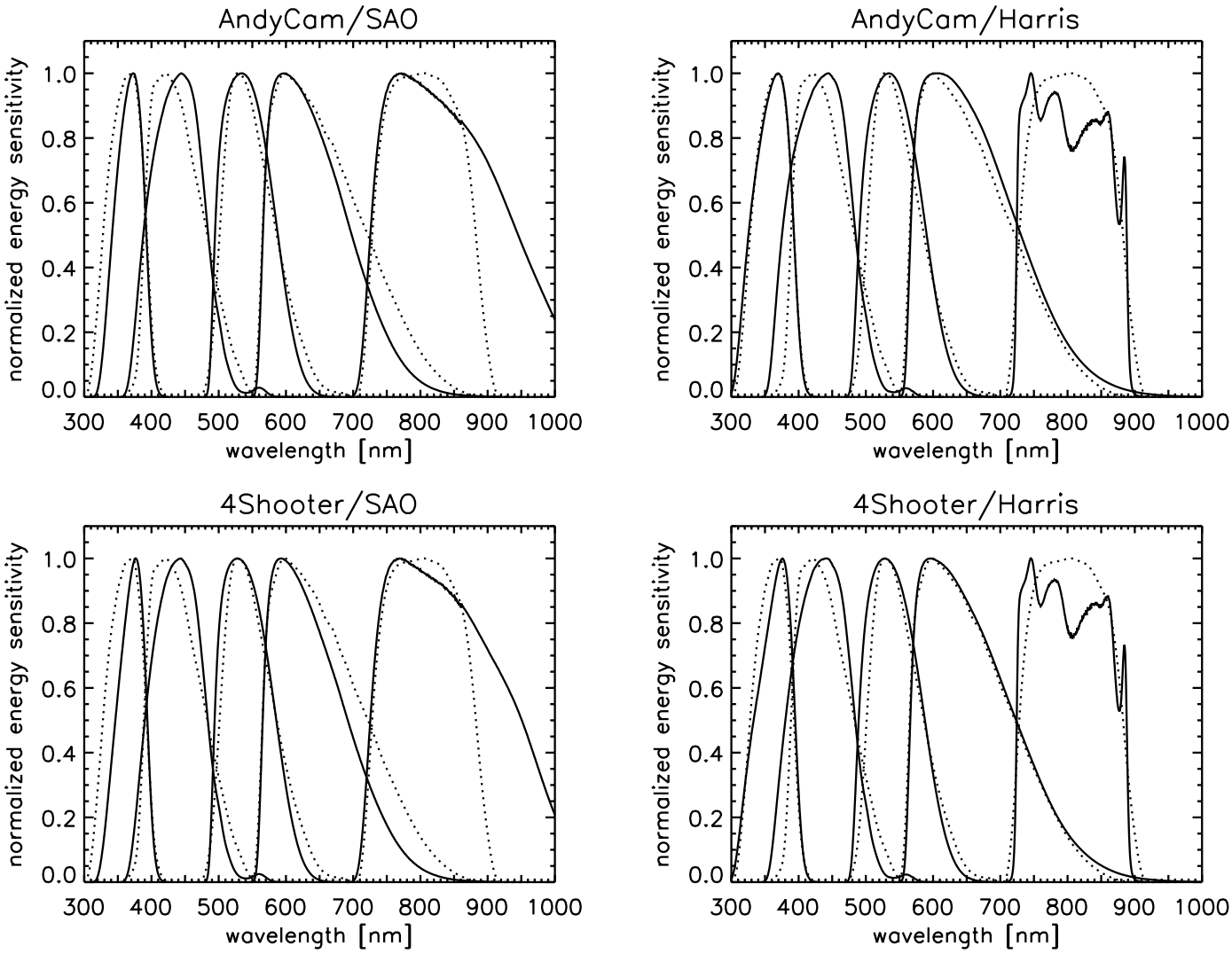

FIG. 3.—Synthesized natural system *UBVRI* passbands (*solid curves*) with the standard *UX* and *BVRI* passbands (*dotted curves*) of Bessell (1990) shown for each detector–filter set combination.

TABLE 5

NATURAL SYSTEM *UBVRI* PASSBANDS

WAVELENGTH (nm)	DETECTOR/FILTER SET NORMALIZED RESPONSE			
	AndyCam/SAO	AndyCam/Harris	4Shooter/SAO	4Shooter/Harris
		U		
295.....	0.000	0.000	0.000	0.000
300.....	0.000	0.011	0.000	0.009
305.....	0.000	0.060	0.000	0.048
310.....	0.000	0.149	0.000	0.117
315.....	0.002	0.264	0.002	0.206
320.....	0.023	0.381	0.018	0.296
325.....	0.089	0.493	0.067	0.382
330.....	0.194	0.592	0.148	0.459
335.....	0.326	0.673	0.250	0.527
340.....	0.465	0.745	0.362	0.591

NOTES.—Table 5 is published in its entirety in the electronic edition of the *Astronomical Journal*. A portion is shown here for guidance regarding its form and content.

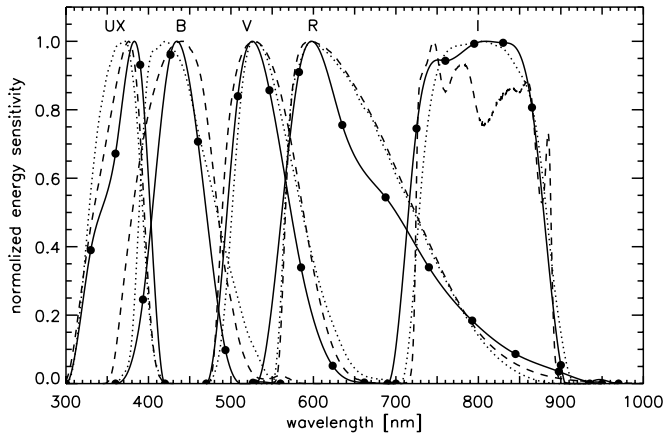

FIG. 4.—Model 4Shooter Harris *UBVRI* passbands derived from observations of spectrophotometric standard stars (*solid curves*), calculated passbands from optics + filter transmission + detector response (*dashed curves*), and the standard *UX* and *BVRI* passbands of Bessell (1990; *dotted curves*). The filled circles show the locations of the model spline points; see text for details.

avoiding pathological cases and overfitting the measurements at the expense of detailed information about the shape of the response curve. We have also imposed constraints that the model passband is "reasonable"; it is forced to zero at the ends and not allowed to be wildly oscillatory.

Given these constraints, the best-fit model passbands from the spectrophotometric data are shown in Figure 4, along with the 4Shooter Harris passbands synthesized from the CCD QE curves, filter transmissions, etc., from Figure 3, and the Bessell (1990) passbands. Because of the somewhat arbitrary nature of the model, as well as uncertainties in the photometry, these best-fit response curves should be viewed as "typical" realizations of the true response rather than exact representations. There is a range of models that fit the data reasonably well (with a dispersion of $\sim$0.02 mag in *BVRI* and $\sim$0.04 mag in *U*, similar to the scatter typically exhibited by the Landolt standards), and this range overlaps well with the calculated passbands. A few of the discrepancies between the solid and dashed curves seem to be robust; in particular, the spectrophotometric data favor a *B* response, which is narrower than the filter transmission would predict. To test this definitively, we would need a larger data set, with more spectrophotometric standards.

Although we have only tried this exercise with one detector–filter set combination, the results suggest that the match between the best-fit model passband and the calculated passbands is generally good, with the calculated passband yielding photometry always within 2 σ of the best fit. Furthermore, the constancy of the color terms for a particular detector–filter set indicates that variable detector response or mirror reflectivity (due to cleanliness, for instance) do not significantly affect the natural system bandpasses. We thus conclude that the response curves shown in Figure 3 and Table 5 are good representations of the natural system.

3. RESULTS

3.1. *Comparison with Published Photometry*

A number of the SNe presented here have published photometry from other groups. Because of the difficulties in SN photometry (correcting for galaxy contamination, transformation to the standard system, etc.), systematic differences between SN photometry from different telescopes are common. These differences are generally small, at the level of a few hundredths of a magnitude (see, e.g., Suntzeff et al. 1999; Jha et al. 1999; Riess et al. 1999), although larger differences can occur with worse filter mismatches. In this paper we strive to present photometry that is internally as homogeneous as possible, but it is still useful to compare these data with independent observations. When the systematic differences are small, combining these independent data sets is highly desirable, producing dramatic improvements in the light-curve sampling.

3.1.1. *SN 1997bp*

Altavilla et al. (2004) present photometry of 18 SNe Ia from the ESO (La Silla) and Asiago Observatory, including four objects also presented here. For SN 1997bp in NGC 4680, the two data sets are quite complementary in the SN phase, with the Altavilla et al. photometry filling in a gap in our light curve just after maximum light. Based on the few contemporaneous points, the photometry shows good agreement in *BVRI*, with offsets $\lesssim$0.05 mag. However, the *U*-band photometry is more discordant; the Altavilla et al. measurements of SN 1997bp are $\sim$0.15 mag fainter in *U* than the photometry presented here.

3.1.2. *SN 1997br*

Li et al. (1999) present extensive *BVRI* photometry of SN 1997br in ESO 576-40 from observations at the Beijing Astronomical Observatory 0.6 m telescope and the Lick Observatory 0.76 m Katzman Automatic Imaging Telescope (KAIT). There is good agreement in the *V*- and *I*-band photometry presented by Li et al. and that presented here (rms offsets $\lesssim$0.05 mag), but there are larger systematic differences in *B* (an rms offset of 0.08 mag, with the Li et al. photometry fainter before maximum light but brighter at later times, $\gtrsim$30 days after maximum light). The most significant discrepancy is in the *R* photometry, for which the Li et al. photometry is fainter than the FLWO photometry by $\sim$0.18 mag on average, approaching $\sim$0.25 mag even near maximum light. The field comparison stars we have in common show good agreement.[4] However, the color terms presented by Li et al. are relatively large in *R*, e.g., $(v - r)/(V - R) = 1.20$ for the KAIT observations, and the photometry differences correlate well with the SN color, implying that the transformation to the standard system is the likely culprit.

Altavilla et al. (2004) report three epochs of *BVRI* photometry of SN 1997br, and these show good agreement ($\lesssim$0.05 mag) with the FLWO photometry presented here (also showing a similar offset when compared to the Li et al. *R*-band data). Altavilla et al. also present two *U*-band points, in fairly good accord ($\lesssim$0.1 mag) with the FLWO photometry.

3.1.3. *SN 1997cn*

Turatto et al. (1998) present *UBVRI* photometry of SN 1997cn in NGC 5490 from a number of telescopes at ESO, La Silla. Our photometry agrees well with theirs in *B* and *V*; in *U* our photometry is generally brighter by $\sim$0.15 mag but is consistent within the photometric uncertainties for this faint object. Our *R*- and *I*-band photometry is also brighter, by $\sim$0.08 mag. We have one comparison star in common with Turatto et al. (their star 2 is our star 9), and our photometry for this star agrees within the reported uncertainties in all bands.

[4] The finder chart presented by Li et al. (1999) seems to indicate that their star E corresponds to our comparison star 6, but the photometry in their Table 1 matches our photometry of comparison star 5, which is somewhat fainter and much redder than star 6. Because of its faintness, Li et al. do not assign much weight to this star, so it is unlikely to explain the discrepant *R* magnitudes.

3.1.4. *SN 1998de*

Extensive *BVRI* observations of SN 1998de in NGC 252 are presented by Modjaz et al. (2001). The data presented there have been *K*-corrected to the SN rest frame, and to facilitate direct comparison with our observations, M. Modjaz has kindly supplied us with their standard magnitudes before *K*-correction. Our data set is relatively sparse compared to that presented by Modjaz et al.,[5] but the agreement is very good before maximum light ($\lesssim$0.05 mag). Our *I*-band data taken about 45 days past maximum light show a large discrepancy ($\sim$0.4 mag), likely a result of the transformation to the standard system at a phase when the SN spectrum is highly nonstellar. Comparison star C of Modjaz et al. is the same as our star 8, and our calibration is consistent.

3.1.5. *SN 1999aa*

Krisciunas et al. (2000) present *BVRI* observations of SN 1999aa in NGC 2595 that very nicely complement the data presented here. In addition, the photometric agreement is superb, with rms offsets $\lesssim$0.03 mag near maximum light and $\lesssim$0.06 mag at late times. Combining the data sets yields an excellent light curve for this object.

Altavilla et al. (2004) present three epochs of *UBVRI* photometry of SN 1999aa, with good accord in *BVR* at the level of $\sim$0.04 mag and larger discrepancies in *I* ($\sim$0.1 mag at 30 days past maximum light and $\sim$0.2 mag at 60 days past maximum light). The *U*-band agreement is also good: $\sim$0.05 mag at +30 days and $\sim$0.1 mag at +60 days.

3.1.6. *SN 1999cl*

Krisciunas et al. (2000) also present *BVRI* observations of the nearby SN 1999cl in NGC 4501 (M88). The data are not as extensive as for SN 1999aa, nor is the photometric agreement as good. The two sets agree relatively well in all bands at maximum light ($\sim$0.03 mag), but the photometry of Krisciunas et al. at about a month past maximum is brighter than our (single) late-time point at that epoch by 0.1–0.3 mag in the different bands. Moreover, the discrepancy is larger in the red. This is a good indication of contamination from the host galaxy; indeed, Krisciunas et al. note that SN 1999cl might be an object for which galaxy subtraction would improve their aperture photometry performed without a template. Our late-time images after the SN had faded show that the host galaxy makes a nonnegligible contribution to the flux at the position of the SN. Based on this discrepancy, Krisciunas et al. have reanalyzed their data for SN 1999cl with subtraction of host-galaxy template images, and the new results bring the photometry into much better agreement (K. Krisciunas 2002, private communication).

3.1.7. *SN 1999ek*

Extensive *BVRI* photometry of SN 1999ek in UGC 3329 is provided by Krisciunas et al. (2004), supplemented by the handful of data points presented here. Comparing the one epoch common to both data sets shows good agreement ($\sim$0.05 mag) in *B* and *I*, as well as excellent agreement ($\sim$0.01 mag) in *V* and *R*. In addition, Krisciunas et al. list *BVRI* magnitudes for two of the field comparison stars we have used, with excellent agreement ($\sim$0.01 mag) in all bands.

3.1.8. *SN 1999gp and SN 2000ce*

Krisciunas et al. (2001) present *BVRI* photometry of five SNe Ia, including SN 1999gp in UGC 1993 (with galaxy subtraction) and SN 2000ce in UGC 4195. For SN 1999gp, the two sets of photometry match extremely well ($\lesssim$0.03 mag), with only a small ($\sim$0.05 mag) consistent difference in the *R*-band photometry. This discrepancy can be traced directly to the comparison stars, as the ones in common show an identical offset. Our comparison star photometry for the SN 1999gp field comes from five photometric nights, with consistent *R* photometry at all epochs. We thus recommend that the Krisciunas et al. SN 1999gp *R* photometry be adjusted 0.05 mag brighter to be consistent with the data presented here. As in the case of SN 1999aa, the data sets are nicely complementary.

The light curve of SN 2000ce also benefits from the combined data sets. In fact, the overlap is very slight (we have two epochs in common, and only one for all the bands simultaneously). Nonetheless, the agreement of the photometry at these epochs is good ($\lesssim$0.04 mag).

3.1.9. *SN 2000cx*

Li et al. (2001) and Candia et al. (2003) present an immense data set in *UBVRI* for the unique SN 2000cx in NGC 524, with an additional two epochs of *UBVRI* reported in Altavilla et al. (2004). The photometry presented here is also quite extensive, except for the fact that the SN was discovered in mid-July, just prior to the aforementioned August shutdown of FLWO. Thus, our data set consists only of one set of points near maximum light, before a large number of observations beginning a month later. The data taken together comprise the most optical photometry of any SN Ia and generally show good photometric agreement, at the level of $\sim$0.05 mag, as far as 100 days past maximum light (see Fig. 3 of Candia et al.). At even later times, the agreement is still generally good, although there are some larger discrepancies, worst in the *I* band, in which the FLWO data and the KAIT data of Li et al. differ by $\sim$0.4 mag. Candia et al. provide more detailed comparisons of subsets of this large data set.

Although we have described photometric agreement from different telescopes at the level of $\lesssim$0.05 mag as "good," it nonetheless remains the case that these differences are systematic and often exceed the nominal published uncertainties. The problem is almost certainly caused by variations in the photometric passbands at different sites that cannot be corrected by a simple linear transformation based on a broadband color. Some of these discrepancies can be overcome by corrections derived from direct application of instrumental passbands to SN spectrophotometry (e.g., Jha et al. 1999). Stritzinger et al. (2002) have formalized this idea through "*S*-corrections," determined in analogy to *K*-corrections. However, the calculated *S*-corrections have not always proved effective in reconciling discordant photometry. In addition, accurate *S*-corrections require accurate knowledge of both instrumental bandpasses and SN spectrophotometry, neither of which are always available. These issues in combining photometry from different sites are compounded in cosmological applications of SNe Ia over a wide range of redshifts and will be an important source of systematic uncertainty that must be controlled in the era of precision cosmology.

3.2. *SN and Host Galaxy Properties*

In Table 6 we list basic data about each SN Ia. The host-galaxy heliocentric redshifts listed are taken from the Updated Zwicky Catalog (Falco et al. 1999) if possible, and from the NASA/IPAC Extragalactic Database[6] (NED) otherwise, where we favor optical redshifts over H I redshifts if there is a discrepancy. For three objects, host-galaxy redshifts were not available, and we

[5] This is due to the fact that the SN peaked at the end of July, just as FLWO undergoes a month-long shutdown because of the southern Arizona monsoons.

[6] The NED is operated by the Jet Propulsion Laboratory, California Institute of Technology, under contract with the National Aeronautics and Space Administration.

TABLE 6
SN Ia and Host Basic Data

SN Ia	Host Galaxy	$cz_{\rm helio}$ (km s^{-1})	Morphology	SN Offsets (arcsec) North	SN Offsets (arcsec) East	$E(B-V)_{\rm Gal}$ (mag)
1997E	NGC 2258	4001	S0	+57	−32	0.124
1997Y	NGC 4675	4806	Sb	+2	−8	0.017
1997bp	NGC 4680	2492	Sd/Irr	−20	−15	0.044
1997bq	NGC 3147	2780	Sbc	−60	+50	0.024
1997br	ESO 576-40	2085	Sd/Irr	+52	−21	0.113
1997cn	NGC 5490	4855	E	−12	+7	0.027
1997cw	NGC 105	5133	Sab	+4	+8	0.073
1997dg	Anonymous	9238	...	0	+2	0.078
1997do	UGC 3845	3034	Sbc	−4	−3	0.063
1997dt	NGC 7448	2194	Sbc	+1	−9	0.057
1998D	NGC 5440	3765	Sa	−7	−26	0.015
1998V	NGC 6627	5268	Sb	+21	−21	0.196
1998ab	NGC 4704	8134	Sc	+12	+2	0.017
1998bp	NGC 6495	3127	E	+13	−1	0.076
1998co	NGC 7131	5418	S0	+5	+2	0.043
1998de	NGC 252	4990	S0	+3	+72	0.057
1998dh	NGC 7541	2678	Sbc	+10	−54	0.068
1998dk	UGC 139	3963	Sc	+3	+5	0.044
1998dm	MCG −01-4-44	1968	Sc	−37	−14	0.044
1998dx	UGC 11149	16197	Sb	−12	+21	0.041
1998ec	UGC 3576	5966	Sb	−20	−9	0.085
1998ef	UGC 646	5319	Sa	−2	+6	0.073
1998eg	UGC 12133	7423	Sc	−25	−26	0.123
1998es	NGC 632	3168	S0	+11	0	0.032
1999X	CGCG 180-22	7503	...	+6	+4	0.032
1999aa	NGC 2595	4330	Sc	+28	+1	0.040
1999ac	NGC 6063	2848	Scd	−30	+24	0.046
1999cc	NGC 6038	9392	Sc	+2	+17	0.023
1999cl	NGC 4501 (M88)	2281	Sb	+23	−46	0.038
1999cw	MCG −01-02-001	3725	Sab	−2	+21	0.036
1999dq	NGC 976	4295	Sc	−6	−4	0.110
1999ef	UGC 607	11733	Scd	−10	+20	0.087
1999ej	NGC 495	4114	S0/Sa	−20	+18	0.071
1999ek	UGC 3329	5253	Sbc	−12	−12	0.561
1999gd	NGC 2623	5535	...	+17	+7	0.041
1999gh	NGC 2986	2302	E	+16	+52	0.058
1999gp	UGC 1993	8018	Sb	+10	−11	0.056
2000B	NGC 2320	5901	E	+19	−14	0.068
2000ce	UGC 4195	4888	Sb	+17	+15	0.057
2000cf	MCG +11-19-25	10920	...	+4	+3	0.032
2000cn	UGC 11064	7043	Scd	−7	−7	0.057
2000cx	NGC 524	2379	S0	−109	−23	0.082
2000dk	NGC 382	5228	E	+9	−5	0.070
2000fa	UGC 3770	6378	Sd/Irr	+4	+7	0.069

report them here based on spectroscopy with the FLWO 1.5 m telescope plus FAST (Fabricant et al. 1998) and cross-correlation with galaxy templates: the host of SN 1997dg, with $cz_{\rm helio} = 9238 \pm 14$ km s^{-1}; the host of SN 1998dx (UGC 11149), with $cz_{\rm helio} = 16,197 \pm 32$ km s^{-1}; and the host of SN 2000cf (MCG +11-19-25), with $cz_{\rm helio} = 10{,}920 \pm 20$ km s^{-1}.

The SNe in the sample range from heliocentric redshifts of 1968 to 16,197 km s^{-1}, with median and mean redshifts of 4888 and 5274 km s^{-1}, respectively. The mean redshift is significantly less than both the original CfA sample of Riess et al. (1999; $\overline{cz} \simeq 7500$ km s^{-1}) and the Calán/Tololo sample of Hamuy et al. (1996b; $\overline{cz} \simeq 13,500$ km s^{-1}). Nonetheless, most of the objects are in the Hubble flow; 39 of the 44 SNe Ia have $cz \geq 2500$ km s^{-1} in the cosmic microwave background rest frame, a slightly larger fraction than the original CfA sample (17 out of 22).

The host-galaxy morphology information shown in Table 6 is taken from the NED, and the SN offset from the nucleus is taken from the IAU CBAT list of SNe.[7] Gallagher et al. (2005) present an analysis of correlations between these properties and SN luminosity. In Table 6 we also list the Galactic reddening toward each SN, derived from the dust maps of Schlegel et al. (1998).

3.3. *Light-Curve Properties*

In Table 7 we list the times of maximum light in B for each SN, as determined from either a direct polynomial fit to the B light curve or from MLCS2k2 fits (Jha et al. 2005). We also present the epoch of the first observation in our data set (measured in the SN rest frame). Over half the objects (25 out of 44)

[7] See http://cfa-www.harvard.edu/iau/lists/Supernovae.html.

TABLE 7
LIGHT-CURVE DATA AND $\Delta m_{15}(B)$ TEMPLATE FITS

SN Ia	$HJD_{B_{max}}$	FIRST OBSERVATION	$\Delta m_{15}(B)$ FITS			
			$\Delta m_{15}(B)$	$B_{B_{max}}$	$V_{B_{max}}$	$I_{B_{max}}$
1997E	2,450,468.0	−3.1	1.39 ± 0.06	15.59	15.47	15.50
1997Y	2,450,487.5	1.4	1.25 ± 0.10	15.28	15.31	15.39
1997bp	2,450,550.3	−3.5	1.00 ± 0.05	14.15	13.89	14.10
1997bq	2,450,558.5	−10.8	1.01 ± 0.05	14.57	14.27	14.38
1997br	2,450,559.7	−7.8	1.02 ± 0.06	14.02	13.61	13.45
1997cn	2,450,583.9	13.6	1.90 ± 0.05	16.93	16.44	16.24
1997cw	2,450,627.1	15.6	1.02 ± 0.10	16.00	15.52	15.34
1997dg	2,450,722.6	−1.6	1.13 ± 0.09	17.20	17.11	17.16
1997do	2,450,767.0	−7.0	0.99 ± 0.10	14.56	14.46	14.60
1997dt	2,450,786.6	−8.9	1.04 ± 0.15	15.64	15.08	14.55
1998D	2,450,841.2	32.4	...	...	...	...
1998V	2,450,891.1	2.9	1.06 ± 0.05	15.88	15.71	15.63
1998ab	2,450,915.2	−8.2	0.88 ± 0.17	15.94	15.93	15.99
1998bp	2,450,936.4	−1.5	1.83 ± 0.06	15.73	15.29	15.09
1998co	2,450,987.2	3.7	...	...	...	...
1998de	2,451,026.2	−4.2	1.93 ± 0.05	17.55	16.83	16.58
1998dh	2,451,030.0	−8.0	1.23 ± 0.17	14.24	13.99	14.07
1998dk	2,451,056.8	18.7	1.05 ± 0.10	14.93	14.74	14.82
1998dm	2,451,061.2	10.5	1.07 ± 0.06	14.70	14.48	14.29
1998dx	2,451,072.6	0.0	1.55 ± 0.09	17.71	17.76	17.90
1998ec	2,451,088.6	13.1	1.08 ± 0.09	16.44	16.21	16.23
1998ef	2,451,114.5	−7.7	0.97 ± 0.10	15.21	15.18	15.29
1998eg	2,451,111.4	−0.7	1.15 ± 0.09	16.62	16.50	16.51
1998es	2,451,143.4	−9.4	0.87 ± 0.08	13.99	13.87	14.12
1999X	2,451,206.0	11.5	1.11 ± 0.08	16.45	16.29	16.32
1999aa	2,451,233.0	−9.9	0.85 ± 0.08	14.91	14.91	15.25
1999ac	2,451,251.2	−4.2	1.00 ± 0.08	14.34	14.28	14.33
1999cc	2,451,315.5	−2.5	1.46 ± 0.05	16.85	16.85	17.08
1999cl	2,451,342.2	−6.5	1.19 ± 0.19	15.11	13.90	13.10
1999cw	2,451,355.9	20.8	...	...	...	...
1999dq	2,451,436.7	−9.5	0.88 ± 0.08	14.88	14.68	14.77
1999ef	2,451,457.7	6.9	1.06 ± 0.05	17.52	17.39	17.70
1999ej	2,451,483.7	4.0	1.41 ± 0.05	15.65	15.63	15.71
1999ek	2,451,481.6	6.2	1.13 ± 0.09	17.97	17.19	16.56
1999gd	2,451,518.5	3.4	1.16 ± 0.06	17.02	16.61	16.29
1999gh	2,451,510.4	10.4	1.69 ± 0.05	14.46	14.27	14.27
1999gp	2,451,551.1	−5.1	0.87 ± 0.08	16.25	16.12	16.44
2000B	2,451,564.8	13.8	1.46 ± 0.05	15.94	15.80	15.99
2000ce	2,451,667.6	6.9	1.06 ± 0.10	17.39	16.71	16.23
2000cf	2,451,674.4	2.4	1.27 ± 0.12	17.15	17.12	17.34
2000cn	2,451,707.5	−7.5	1.58 ± 0.12	16.82	16.64	16.71
2000cx	2,451,752.2	−0.2	...	...	...	...
2000dk	2,451,812.5	−4.5	1.57 ± 0.09	15.63	15.57	15.77
2000fa	2,451,892.7	−10.5	1.00 ± 0.10	15.99	15.95	16.13

have observations before maximum light, and 70% (31 out of 44) have observations earlier than 5 days past maximum light.

We have also fitted the *BVI* light curves of our SN sample to determine maximum light magnitudes and the parameter $\Delta m_{15}(B)$, which has been shown to correlate with the SN intrinsic luminosity (Phillips 1993). Although originally defined as the measured decline rate of the SN in B from maximum to 15 days past maximum light, we follow Hamuy et al. (1995, 1996b), who define $\Delta m_{15}(B)$ as a parameter in a multidimensional fit to template light curves [each with a predefined $\Delta m_{15}(B)$]. We have followed the recipe of Hamuy et al. (1996b) in our fits, using a parabolic fit through the minimum reduced χ^2 in a fit of the *BVI* light curves to each of a set of templates ("de-K-corrected" and time dilated to the observer's frame for each SN). We have used the six *BVI* templates presented by Hamuy et al. (1996a) and augmented this sample with templates based on an additional four well-observed SNe Ia in order to produce more robust measurements of $\Delta m_{15}(B)$: SN 1995al [$\Delta m_{15}(B) = 0.83$; Riess et al. 1999], SN 1998aq [$\Delta m_{15}(B) = 1.13$; Riess et al. 2005], SN 1998bu [$\Delta m_{15}(B) = 1.01$; Suntzeff et al. 1999; Jha et al. 1999], and SN 1999by [$\Delta m_{15}(B) = 1.90$; Garnavich et al. 2004]. We were able to get reliable $\Delta m_{15}(B)$ measurements for all but four of the SNe Ia;[8] these values (not corrected for host-galaxy reddening) and their uncertainties (estimated from the curvature of the best-fit parabola) are listed in Table 7. We also present the *BVI* magnitudes at maximum light (in B) for each SN determined from the best-fit template.

[8] The four objects include SN 1998D and SN 1999cw, for which the first observations were well after maximum light; SN 1998co, for which the data are quite sparse; and SN 2000cx, whose light curve is unique among all SNe Ia (Li et al. 2001).

TABLE 8
UBV Stretch Template Fits

SN Ia	$U_{B_{\max}}$	$B_{B_{\max}}$	$V_{B_{\max}}$	s_U	s_B	s_V	$t_U - t_B$	$t_V - t_B$	χ^2/dof
1997E	15.40 ± 0.05	15.62 ± 0.02	15.47 ± 0.02	0.79 ± 0.04	0.83 ± 0.02	0.87 ± 0.03	−1.8 ± 0.8	0.7 ± 0.3	2.3
1997Y	14.90 ± 0.07	15.35 ± 0.08	15.39 ± 0.02	0.96 ± 0.08	0.93 ± 0.03	0.91 ± 0.04	−1.9 ± 1.3	1.6 ± 0.7	0.2
1997bp	14.05 ± 0.05	14.10 ± 0.02	13.91 ± 0.02	1.12 ± 0.03	0.97 ± 0.03	1.07 ± 0.03	−3.1 ± 1.0	2.1 ± 0.4	2.3
1997bq	14.23 ± 0.04	14.53 ± 0.02	14.44 ± 0.02	0.89 ± 0.02	0.92 ± 0.02	1.02 ± 0.02	−2.1 ± 0.2	1.6 ± 0.1	0.7
1997br	13.29 ± 0.12	13.88 ± 0.05	13.62 ± 0.02	0.81 ± 0.05	0.91 ± 0.03	1.04 ± 0.03	−2.6 ± 0.4	1.1 ± 0.2	2.1
1998V	15.62 ± 0.07	15.91 ± 0.04	15.73 ± 0.03	0.89 ± 0.07	0.99 ± 0.05	0.96 ± 0.04	−1.8 ± 1.8	0.7 ± 0.9	4.0
1998ab	15.51 ± 0.06	16.08 ± 0.03	16.10 ± 0.02	0.83 ± 0.03	0.92 ± 0.02	1.02 ± 0.02	−2.0 ± 0.2	0.5 ± 0.2	1.1
1998bp	15.56 ± 0.07	15.63 ± 0.02	15.31 ± 0.02	0.71 ± 0.04	0.65 ± 0.02	0.66 ± 0.02	−3.1 ± 1.2	2.1 ± 0.4	2.7
1998dh	13.91 ± 0.06	14.15 ± 0.02	14.04 ± 0.02	0.90 ± 0.03	0.91 ± 0.02	0.98 ± 0.02	−1.9 ± 0.3	1.1 ± 0.2	0.7
1998dx	17.02 ± 0.13	17.69 ± 0.05	17.74 ± 0.03	0.70 ± 0.06	0.85 ± 0.04	0.81 ± 0.04	−2.0 ± 1.3	1.2 ± 0.7	1.4
1998eg	16.20 ± 0.06	16.61 ± 0.02	16.50 ± 0.02	0.88 ± 0.06	0.96 ± 0.04	0.98 ± 0.04	−2.3 ± 0.9	1.3 ± 0.6	0.6
1998es	13.45 ± 0.04	13.97 ± 0.02	13.87 ± 0.01	0.98 ± 0.03	1.13 ± 0.02	1.10 ± 0.02	−1.6 ± 0.3	0.4 ± 0.2	1.0
1999aa	14.37 ± 0.04	14.89 ± 0.03	14.94 ± 0.02	1.05 ± 0.02	1.11 ± 0.03	1.13 ± 0.02	−2.2 ± 0.3	0.0 ± 0.2	2.9
1999ac	14.03 ± 0.06	14.28 ± 0.03	14.22 ± 0.02	1.04 ± 0.04	0.93 ± 0.05	0.99 ± 0.02	−2.7 ± 0.9	2.0 ± 0.4	4.0
1999cc	16.60 ± 0.06	16.88 ± 0.03	16.89 ± 0.02	0.86 ± 0.05	0.81 ± 0.03	0.87 ± 0.03	−2.0 ± 0.9	0.3 ± 0.5	1.8
1999cl	15.76 ± 0.05	15.07 ± 0.03	13.88 ± 0.02	0.82 ± 0.04	0.97 ± 0.04	1.02 ± 0.03	−1.9 ± 0.6	1.7 ± 0.4	0.5
1999dq	14.43 ± 0.04	14.86 ± 0.02	14.69 ± 0.02	0.98 ± 0.02	1.08 ± 0.02	1.13 ± 0.02	−2.3 ± 0.2	0.3 ± 0.2	1.5
1999gp	15.67 ± 0.07	16.26 ± 0.03	16.19 ± 0.02	1.04 ± 0.07	1.17 ± 0.06	1.20 ± 0.04	−2.0 ± 1.2	0.8 ± 0.6	6.2
2000cf	16.84 ± 0.11	17.18 ± 0.04	17.21 ± 0.02	0.83 ± 0.06	0.87 ± 0.02	0.92 ± 0.03	−2.2 ± 1.3	1.4 ± 0.7	0.6
2000cn	16.76 ± 0.07	16.81 ± 0.03	16.59 ± 0.02	0.76 ± 0.06	0.77 ± 0.03	0.82 ± 0.02	−1.7 ± 0.3	1.2 ± 0.2	2.3
2000dk	15.36 ± 0.05	15.63 ± 0.02	15.57 ± 0.02	0.73 ± 0.04	0.74 ± 0.02	0.81 ± 0.03	−2.5 ± 0.5	1.1 ± 0.2	2.7
2000fa	15.82 ± 0.08	16.13 ± 0.04	16.04 ± 0.03	1.01 ± 0.03	1.04 ± 0.03	0.97 ± 0.03	−2.3 ± 1.0	1.4 ± 0.8	1.2

To further explore the light-curve properties of this sample and, in particular, to study the *U*-band light curves, we have also fitted the light curves to templates based on the timescale stretch parameterization developed by the Supernova Cosmology Project (SCP; Perlmutter et al. 1997, 1999; Goldhaber et al. 2001). The stretch template presented by Goldhaber et al. (2001) is only for the *B* band; we would like to fit the *UBV* light curves, for which the simple stretching of the time axis does a good job of fitting the observed data. To construct *U*- and *V*-band templates, one possibility is to use composite light curves, combining a large number of SNe to produce an average template. However, because some objects are better sampled in different bands, the average templates produced this way might not consistently represent a SN of "average" light-curve shape and/or luminosity. For this reason, we have constructed *UBV* templates based on photometry of a single SN, the well-observed SN 1998aq (Riess et al. 2005). To retain consistency with the Goldhaber et al. (2001) normalization, we have corrected our SN 1998aq *UBV* stretch templates to $s = 1$, by fitting the *B* template to the SCP 1997 template presented in that paper.

In fitting our stretch templates to the data, we generally follow the methodology of Goldhaber et al. (2001) as applied in their analysis of the Calán/Tololo sample (Hamuy et al. 1996b). We restrict the light curves to between −10 and +40 days in the SN rest frame, and we only include objects with photometry commencing earlier than 5 days after maximum light. Because we are interested in understanding the general light-curve properties of these SNe Ia, we allow the fits to be as unrestrictive as possible: we fit for the stretch individually in each of the three bands and allow the times of maxima to vary in each band (plus or minus a few days), as well as individually fitting for the *UBV* peak magnitudes.[9] We also impose an error floor on the photometry equal to 0.007 times the peak flux, as did Goldhaber et al. (2001; see their Table 7); while this is negligible near maximum, it becomes the dominant uncertainty in the photometry at late times (for instance, corresponding to ±0.2 mag in the *U* band at +40 days). As in the $\Delta m_{15}(B)$ fits above, we fit the data in the observer's frame (de-*K*-correcting and time dilating the templates).

The limits on the epoch of first observation, and the requirement that we need $\gtrsim$5 points between −10 and +40 days in each of the three bands for a meaningful fit, limits the application of this method to 22 of the 44 SNe Ia presented here. The results are presented in Table 8, listing the *UBV* peak magnitudes and timescale stretch factors, along with the differences in the time of maximum light in *U* and *V* relative to $t_{B_{\max}}$, all with error estimates given by the formal uncertainties in the fit.

4. DISCUSSION: *U*-BAND LIGHT CURVES

The *U*-band photometry presented here, while just a fraction of the whole data set, is the first large sample of homogeneously observed and reduced *U* photometry of SNe Ia. The *BVRI* properties of SNe Ia are well studied, and while our data provide a much expanded sample of *BVRI* light curves, here we focus on the new element, the *U*-band data. Although a number of other SNe Ia individually also have published *U*-band photoelectric or CCD photometry, the difficulties of transforming this photometry (with the variety of instruments, filters, sensitivities, etc.; see, e.g., Schaefer 1995; Suntzeff et al. 1999) to a standard system leads us first to examine the *U*-band properties of SNe Ia from FLWO observations alone, as we have taken care to ensure internal consistency.

Figure 5 shows the composite *U*-band light curve of the 44 SNe Ia presented in this paper, along with six other SNe Ia with *U*-band data from the FLWO 1.2 m: SN 1995al and SN 1996X (for which *BVRI* light curves were presented by Riess et al. 1999), SN 1998aq (Riess et al. 2005), SN 1998bu (Jha et al. 1999), SN 1999by (Garnavich et al. 2004), and SN 2001V (K. Mandel et al. 2006, in preparation). Of the *UBVRI* passbands, the SN Ia

[9] We fitted the data in magnitude space rather than flux space out of convenience. Because we are only fitting the light curves between −10 and +40 days, the difference between the two approaches is negligible. Determining rise-time information at very early epochs clearly benefits from fitting in flux space, where negative and zero fluxes are common.

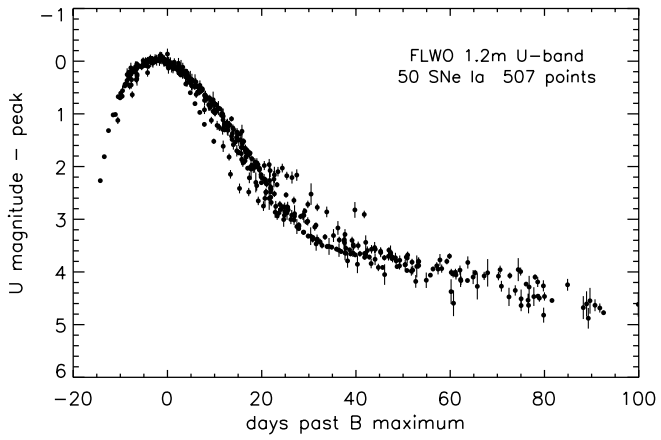

FIG. 5.—Composite *U*-band light curve of 50 SNe Ia observed with the FLWO 1.2 m telescope. The data were *K*-corrected and time dilated to the SN rest frame. There are 507 individual points in the time interval displayed, from −20 to +100 days after maximum light in *B*.

light curve declines fastest in *U*, with an average SN Ia dropping ∼1.5 mag in *U* over the first 15 days after $B_{\max}$, as compared to only an ∼1.1 mag drop in *B* and an ∼0.5 mag drop in *V* over that time period. Over the first 30 days after $B_{\max}$, the declines in *U*, *B*, and *V* are ∼3.2, ∼2.6, and ∼1.4 mag, respectively. At late time, $t \gtrsim 35$ days after *B* maximum light, the *U*-band light curves follow the typical exponential decline, decaying at 0.020 ± 0.001 mag day^{-1}.

In Figure 6 we plot the distribution of the epoch of *U*-band maximum light relative to *B*-band maximum light, using the stretch template results for the 22 SNe Ia listed in Table 8, along with the six additional SNe Ia listed above. As can also be seen in Figure 5, the SNe Ia clearly peak earlier in the *U* band than in *B*, with an average time offset of −2.3 days and a dispersion of only 0.4 days. The earlier peak in *U* also implies that the decline rate in *U* relative to maximum light in *U* is not so different from the decline rate in *B* relative to maximum light in *B*. A typical SN Ia that drops ∼1.1 mag in *B* over the first 15 days after maximum light (as above) declines by ∼1.2 mag in *U* over the first 15 days after *U* maximum. We note that our precise photometry confirms the result of Leibundgut et al. (1991), who found that the maximum in light in *U* occurs ∼2.8 days before maximum light in *B*, based on a compilation of heterogeneous photoelectric *UBV* photometry.

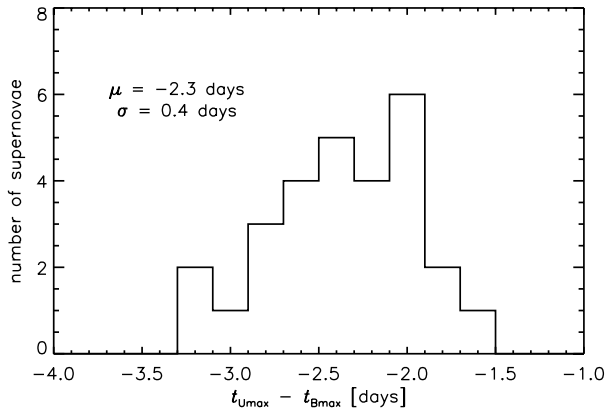

FIG. 6.—Distribution of the time of maximum light in *U* relative to the time of maximum light in *B*, measured in the SN rest frame.

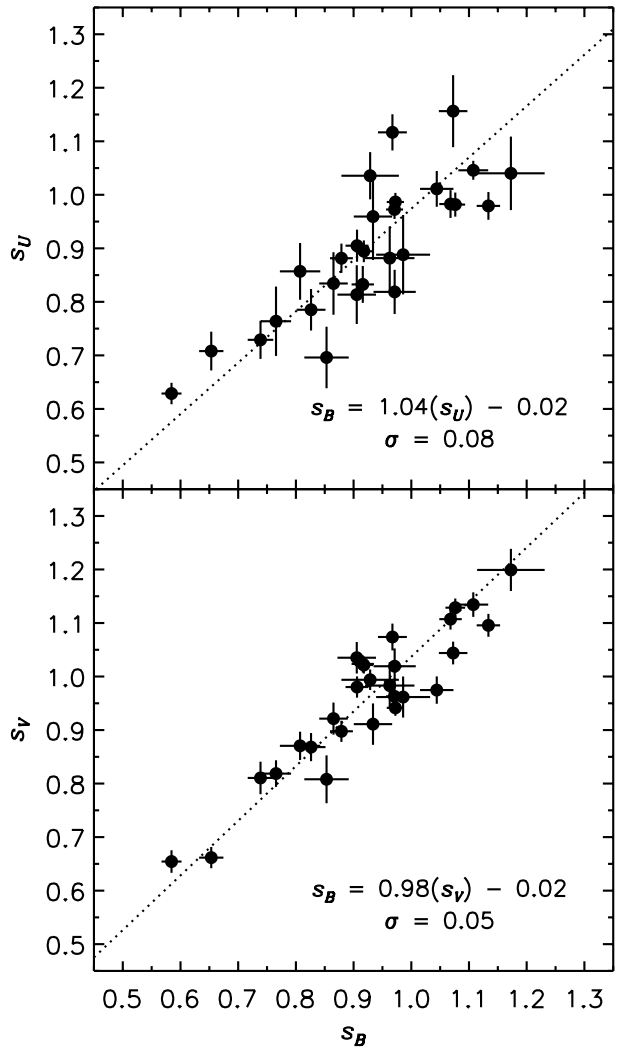

FIG. 7.—Relations between timescale stretch factors in *UBV* based on the stretch-corrected SN 1998aq templates (see text for details). The best linear fits are $s_B = (1.04 \pm 0.06)s_U - (0.02 \pm 0.05)$ and $(0.98 \pm 0.05)s_V - (0.02 \pm 0.05)$.

The decline rate in *U* is well correlated with the decline rate in *B*, as shown in Figure 7, which plots the timescale stretch factors for the 28 SNe Ia described above. However, as the figure also illustrates, there is a significant scatter. The relationship between the stretch factor in *V* and the stretch factor in *B* is considerably tighter. Nonetheless, these correlations imply that *U* light curves can provide leverage in determining the intrinsic luminosities of SNe Ia. The best-fit linear relations between s_U, s_B, and s_V are given in the figure. Given the scatter, the relations are consistent with a "universal" stretch, $s = s_U = s_B = s_V$, although the data for a number of objects individually favor slightly different stretch factors in each band. The slope of the luminosity-stretch relation is ∼1.7 (Nugent et al. 2002), meaning that the dispersion in the s_U-s_B relation ($\sigma \simeq 0.08$) translates into an uncertainty of $\sigma \simeq 0.14$ mag in luminosity, comparable to the typical dispersion in measuring SN Ia distances (e.g., in the stretch-luminosity relation itself). Similarly, the dispersion in the s_V-s_B relation corresponds to $\sigma \simeq 0.09$ mag.

We can also examine the correlation between the timescale stretch factors and $\Delta m_{15}(B)$ for these 28 SNe Ia (see Table 7); the results are shown in Figure 8. The correlation between $\Delta m_{15}(B)$ and *s* is clear, with s_V and s_B producing a tighter relationship. It

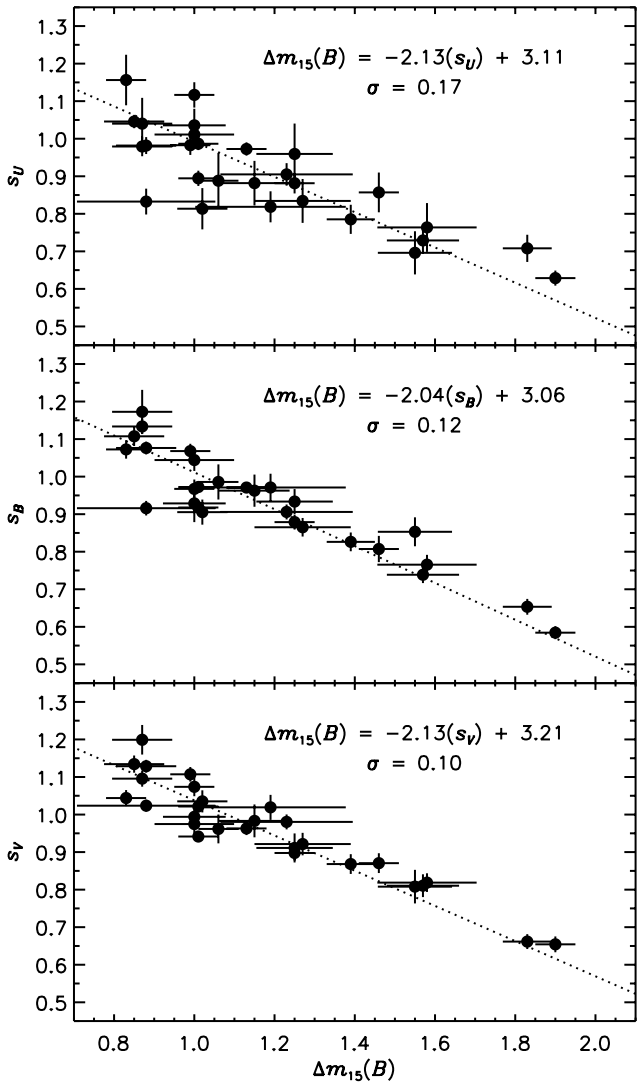

FIG. 8.—Relations between timescale stretch factors and $\Delta m_{15}(B)$. The best linear fits are $\Delta m_{15}(B) = (-2.13 \pm 0.14)s_U + (3.11 \pm 0.13), (-2.04 \pm 0.11)s_B + (3.06 \pm 0.10)$, and $(-2.13 \pm 0.12)s_V + (3.21 \pm 0.11)$.

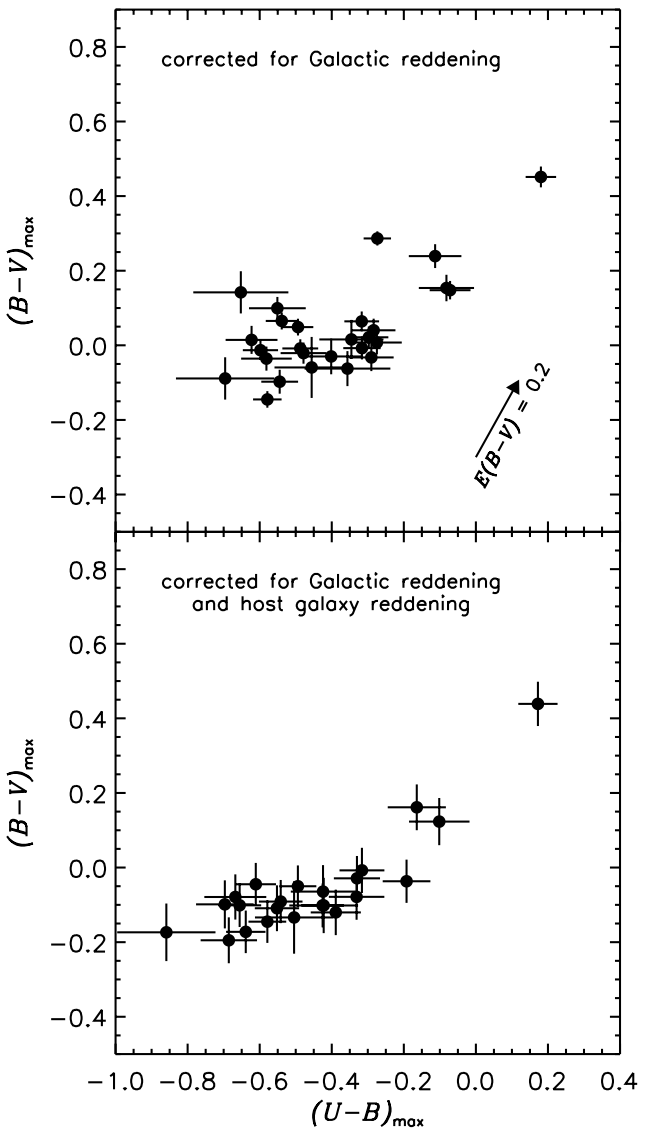

FIG. 9.—SN Ia colors at the epoch of maximum light in *B*. *Top*, Maximum light colors corrected for Galactic extinction; *bottom*, correction for extinction in the host galaxy. The arrow indicates a reddening vector corresponding to $E(B-V)_{\rm true} = 0.2$ mag.

also appears that much of the dispersion comes at the low $\Delta m_{15}(B)$ (large s) end of the diagram, implying that there may be larger intrinsic variation in the light curves of the most luminous SNe Ia. The dispersions in $\Delta m_{15}(B)$ are 0.17, 0.12, and 0.10 for the relations with s_U, s_B, and s_V, respectively. Using the luminosity-$\Delta m_{15}(B)$ relationship presented by Phillips et al. (1999), the luminosity scatter corresponding to these dispersions is 0.14, 0.10, and 0.08 mag, respectively, similar to the results above directly comparing stretch to luminosity. We note that the relations between $\Delta m_{15}(B)$ and s presented in Figure 8 match well the results of Garnavich et al. (2004; see their Fig. 6).

In addition to the *U*-band light-curve shapes, we can explore the $U - B$ color with this data set. We display 27 SNe Ia[10] in the color-color diagram shown in Figure 9 (*top*). We note that the stretch-template fits to the peak magnitudes include the effects of *K*-correction, which can be significant, particularly in the *U* band ($K_{UU} \simeq 0.12$ mag for $z = 0.03$ at maximum light; Jha et al. 2005). We have also corrected the colors for (the generally small) Galactic reddening (Table 6), assuming the $R_V = 3.1$ extinction law of Cardelli et al. (1989). For 23 of the 27 SNe Ia, we were also able to correct for the host-galaxy extinction via measurement of the tail $B - V$ evolution and the method of Lira (1995) and Phillips et al. (1999), as described in detail in Jha et al. (2005). The colors corrected for host-galaxy reddening are shown in Figure 9 (*bottom*). These results sharpen those of Schaefer (1995) and Branch et al. (1997), who display relations between the $U - B$ and $B - V$ maximum light colors of SNe Ia based on a handful of objects with heterogeneous photometry from diverse sources.

Figure 9 (*bottom*) shows a tight relation between the intrinsic $B - V$ and $U - B$ colors at maximum light. In this plot, normal SNe Ia have $B - V \simeq -0.1$ (e.g., Phillips et al. 1999),[11] and

[10] We show 27 SNe Ia rather than 28 because we exclude the highly reddened SN 1999cl for which there is strong evidence from near-infrared photometry that the extinction law varies significantly from the canonical $R_V = 3.1$ law (Krisciunas et al. 2000; Jha et al. 2005).

[11] Phillips et al. (1999) find the "pseudocolor" $B_{B_{\rm max}} - V_{V_{\rm max}} \simeq -0.07$ for normal SNe Ia. Because $V_{V_{\rm max}} \simeq V_{B_{\rm max}} - 0.02$, their result implies $(B - V)_{B_{\rm max}} \simeq -0.09$ for normal SNe Ia.

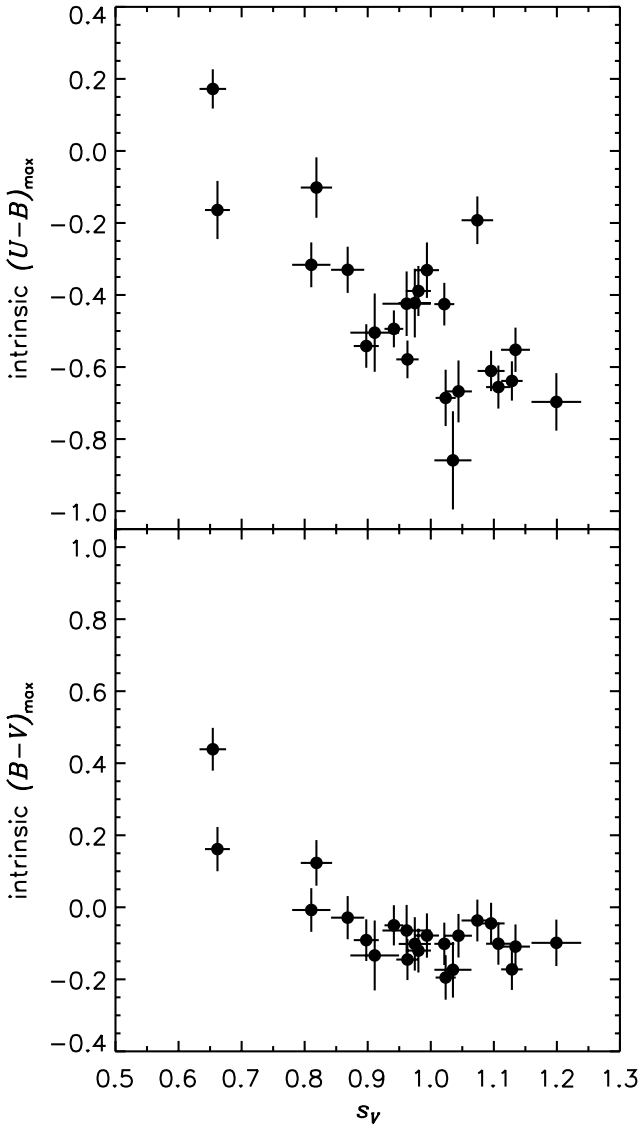

FIG. 10.—Relations between SN Ia *UBV* colors at maximum light in *B* and the *V*-band timescale stretch factor. The colors have been corrected for Galactic and host-galaxy reddening.

there is a strong clustering of objects at this value. Note, however, the wide span of $U - B$ colors (from about -0.2 to -0.8) for these normal SNe Ia. This is not an artifact of the reddening correction, nor can it be explained by variation in the extinction law in these external galaxies. If there were strong variations in the extinction law, the patchiness of interstellar dust would cause Figure 9 (*top*) to show a swarm of points at the lower left (corresponding to an unreddened locus), with the remainder of the points fanning out toward the upper right (corresponding to different amounts of extinction and reddening), which is clearly not what we see. We conclude that the intrinsic variation in $U - B$ color at maximum light is significantly greater than the variation seen in $B - V$.

Do these color variations correlate with light-curve shape or luminosity? There is strong evidence that objects with intrinsically red $B - V$ colors at maximum are fast-declining, low-luminosity SNe Ia (see, e.g., Garnavich et al. 2004 and references therein). Figure 9 (*bottom*) shows that the red objects in $B - V$ are also red in $U - B$. A direct check on the relation between color and light-curve shape is shown in Figure 10, which plots the intrinsic $U - B$ and $B - V$ maximum light colors against the measured timescale stretch factor (in V). The relationship between $B - V$ and s_V shown in the bottom panel is in good accord with the results presented by Phillips et al. (1999) and Garnavich et al. (2004). The $U - B$ results in the top panel show that the $U - B$ color is well correlated with stretch (and therefore luminosity) over the whole range of luminosity in the sample. However, the scatter is also greater in $U - B$, implying that there is a significant intrinsic dispersion in *U*-band peak brightness even after accounting for variations in light-curve shape. A simple linear fit to the data in Figure 10 (*top*) implies that this intrinsic dispersion is $\sigma_U \simeq 0.12$ mag. It would be interesting to check whether this increased dispersion is related to other factors, such as progenitor metallicity, as some theoretical studies have indicated that these factors may have more significant effects in *U* than in *BVRI* (e.g., Höflich et al. 1998).

It is clear that the analysis of these *U*-band light curves and their relation to light curves in *BVRI* and, ultimately, precise distances is intimately tied to the luminosity and extinction of each SN. To further explore these relations, a profitable strategy would be to incorporate the *U*-band light curves into the general framework of the multicolor light curve shape analysis presented by Riess et al. (1996). We present the methods and results of this incorporation in Jha et al. (2005).

We thank the avid supernova searchers who scan the sky and allow us to be successful in finding supernovae in our in-boxes. We are also grateful for the efforts of Dan Green at the IAU CBAT for enabling our follow-up observations. We thank Paul Green, Scott Kenyon, Jeff McClintock, and Kenny Wood for assistance with the observations, Brian Schmidt for robust software, and Adam Riess, Nick Suntzeff, Dimitar Sasselov, and Alyssa Goodman for enlightening discussions and comments. We appreciate the helpful suggestions of the referee, Mario Hamuy, in improving the paper. This work was supported in part by an NSF Graduate Research Fellowship and the Miller Institute for Basic Research in Science. Research on supernovae at Harvard University is supported by NSF grant AST 02-05808.

REFERENCES

Alard, C., & Lupton, R. 1998, ApJ, 503, 325
Altavilla, G., et al. 2004, MNRAS, 349, 1344
Armstrong, M., & Hurst, G. M. 1996, IAU Circ., 6509, 2
Barris, B. J., et al. 2004, ApJ, 602, 571
Bessell, M. S. 1990, PASP, 102, 1181
Bohlin, R. C., Dickinson, M. E., & Calzetti, D. 2001, AJ, 122, 2118
Boisseau, J. R., & Wheeler, J. C. 1991, AJ, 101, 1281
Branch, D., Nugent, P., & Fisher, A. 1997, in Thermonuclear Supernovae, ed. P. Ruiz-Lapuente, R. Canal, & J. Isern (Dordrecht: Kluwer), 715
Candia, P., et al. 2003, PASP, 115, 277
Cardelli, J. A., Clayton, G. C., & Mathis, J. S. 1989, ApJ, 345, 245
Fabricant, D., Cheimets, P., Caldwell, N., & Geary, J. 1998, PASP, 110, 79
Falco, E. E., et al. 1999, PASP, 111, 438
Gallagher, J., Garnavich, P. M., Berlind, P., Challis, P., Jha, S., & Kirshner, R. P. 2005, ApJ, 634, 210
Garnavich, P. M., et al. 2004, ApJ, 613, 1120
Goldhaber, G., et al. 2001, ApJ, 558, 359
Hamuy, M., Phillips, M. M., Maza, J., Suntzeff, N. B., Schommer, R. A., & Avilés, R. 1995, AJ, 109, 1
Hamuy, M., Phillips, M. M., Suntzeff, N. B., Schommer, R. A., Maza, J., Smith, R. C., Lira, P., & Avilés, R. 1996a, AJ, 112, 2438
Hamuy, M., & Pinto, P. A. 1999, AJ, 117, 1185

Hamuy, M., Suntzeff, N. B., Heathcote, S. R., Walker, A. R., Gigoux, P., & Phillips, M. M. 1994, PASP, 106, 566
Hamuy, M., Walker, A. R., Suntzeff, N. B., Gigoux, P., Heathcote, S. R., & Phillips, M. M. 1992, PASP, 104, 533
Hamuy, M., et al. 1993, AJ, 106, 2392
———. 1996b, AJ, 112, 2408
Harris, W. E., Fitzgerald, M. P., & Reed, B. C. 1981, PASP, 93, 507
Höflich, P., Wheeler, J. C., & Thielemann, F. K. 1998, ApJ, 495, 617
Jha, S., Riess, A. G., & Kirshner, R. P. 2005, ApJ, submitted
Jha, S., et al. 1999, ApJS, 125, 73
Knop, R. A., et al. 2003, ApJ, 598, 102
Krisciunas, K., Hastings, N. C., Loomis, K., McMillan, R., Rest, A., Riess, A. G., & Stubbs, C. 2000, ApJ, 539, 658
Krisciunas, K., et al. 2001, AJ, 122, 1616
———. 2004, AJ, 128, 3034
Landolt, A. U. 1992, AJ, 104, 340
Leibundgut, B., Tammann, G. A., Cadonau, R., & Cerrito, D. 1991, A&AS, 89, 537
Li, W. D., Qiu, Y. L., Qiao, Q. Y., Ma, J., & Hu, J. Y. 1996, IAU Circ., 6379, 1
Li, W. D., et al. 1999, AJ, 117, 2709
———. 2001, PASP, 113, 1178
Lira, P. 1995, M.S. thesis, Univ. Chile
Massey, P., & Gronwall, C. 1990, ApJ, 358, 344
Massey, P., Strobel, K., Barnes, J. V., & Anderson, E. 1988, ApJ, 328, 315
Modjaz, M., Li, W. D., Filippenko, A. V., King, J. Y., Leonard, D. C., Matheson, T., & Treffers, R. R. 2001, PASP, 113, 308
Monet, D., et al. 1998, The USNO-A2.0 Catalog (Washington: USNO)
Nugent, P., Kim, A., & Perlmutter, S. 2002, PASP, 114, 803
Perlmutter, S., et al. 1997, ApJ, 483, 565
———. 1999, ApJ, 517, 565
Phillips, M. M. 1993, ApJ, 413, L105
Phillips, M. M., Lira, P., Suntzeff, N. B., Schommer, R. A., Hamuy, M., & Maza, J. 1999, AJ, 118, 1766
Press, W. H., Teukolsky, S. A., Vetterling, W. T., & Flannery, B. P. 1992, Numerical Recipes in C (2nd ed.; New York: Cambridge Univ. Press)
Puckett, T. 1998, IAU Circ., 6957, 1
Riess, A. G., Press, W. H., & Kirshner, R. P. 1996, ApJ, 473, 88
Riess, A. G., et al. 1999, AJ, 117, 707
———. 2004, ApJ, 607, 665
———. 2005, ApJ, 627, 579
Schaefer, B. E. 1995, ApJ, 450, L5
Schechter, P. L., Mateo, M., & Saha, A. 1993, PASP, 105, 1342
Schlegel, D. J., Finkbeiner, D. P., & Davis, M. 1998, ApJ, 500, 525
Schmidt, B. P., et al. 1998, ApJ, 507, 46
Schwartz, M. 1997, IAU Circ., 6700, 1
Stetson, P. 1987, PASP, 99, 191
———. 1994, PASP, 106, 250
Stritzinger, M., et al. 2002, AJ, 124, 2100
Suntzeff, N. B., et al. 1999, AJ, 117, 1175
Treffers, R. R., Peng, C. Y., Filippenko, A. V., Richmond, M. W., Barth, A. J., & Gilbert, A. M. 1997, IAU Circ., 6627, 1
Turatto, M., Piemonte, A., Benetti, S., Cappellaro, E., Mazzali, P. A., Danziger, I. J., & Patat, F. 1998, AJ, 116, 2431